

Limits to the critical transport current in superconducting (Bi,Pb)₂Sr₂Ca₂Cu₃O₁₀ silver-sheathed tapes: The railway-switch model

B. Hensel, G. Grasso,* and R. Flükiger

Université de Genève, Département de Physique de la Matière Condensée, 24, quai Ernest-Ansermet, 1211 Genève 4, Switzerland

(Received 14 November 1994; revised manuscript received 30 January 1995)

We have proposed the “railway-switch” model to describe the superconducting transport current in (Bi,Pb)₂Sr₂Ca₂Cu₃O₁₀ silver-sheathed tapes. The model assumes that in the textured polycrystalline filament the frequent small-angle *c*-axis tilt grain boundaries (“railway switches”) constitute strong links for the supercurrent. With the objective to identify the mechanisms that limit the critical-current density in the tapes we present measurements of the transport critical current normal to the tape plane and of the current-transfer length along the tape axis. From *I-V* curves we obtain the longitudinal critical-current distribution and compare it to the thickness variation of the filament. The experiments have been performed on monofilamentary powder-in-tube samples prepared in long lengths by rolling as the only tape-forming process. For all investigated samples the critical-current density at *T* = 77 K in self-field was in the range $j_c = 20\text{--}30$ kA/cm². We conclude that the dominant limitation for the transport critical current in the tapes is imposed by the low intragrain critical-current density j_c^c along the *c* axis (as compared to the in-plane critical-current density j_c^{ab}) and by the even lower critical-current density j_c^t across twist boundaries or intergrowths. Possibilities for an improvement of the performance of the (Bi,Pb)₂Sr₂Ca₂Cu₃O₁₀ silver-sheathed tapes are discussed.

I. INTRODUCTION

The high-*T_c* superconductor (Bi,Pb)₂Sr₂Ca₂Cu₃O₁₀ [Bi/Pb(2223)] offers promising physical properties for technical applications. The high critical superconducting temperature (*T_c* = 110 K) together with a high critical magnetic field [*B_{c2}*(*T* = 4.2 K) > 100 T] and a potentially high critical-current density j_c promoted the fast development of prototype conductors mainly in the form of silver-sheathed tapes that are generally produced by the “powder-in-tube” (PIT) method. Although being applied to a very complex metallurgical system the PIT process yields reasonable results in a straightforward way and laboratories worldwide participated in the hunt for the record-high critical-current density j_c (*T* = 77 K, *B* = 0 T). This was certainly a decisive stimulus for the rapid progress in the field, besides the promise of future paying applications. However, the pushing of the record value to higher and higher limits was not always accompanied by good reproducibility. Consequently the course of optimizing the tape performance had to change from a diffuse and mainly heuristic research by trial and error with large numbers of samples to a more focused strategy that requires as its base the understanding of the correlation between preparation parameters and technologically relevant properties of the tapes, the most important being for obvious reasons the critical transport current density j_c and its field and temperature dependence $j_c(B, T)$. This change of direction became necessary especially for the development of industrial lengths (*l* > 1 km) of conductors with a restricted variety of production steps and perfect reproducibility being an absolute must.

The first effort in describing the mechanisms of supercurrent transport in Bi/Pb(2223) tapes has been made by

Bulaevskii *et al.*¹ and Malozemoff.² The notion that the platelets in the superconducting filament were stacked like bricks in a wall led them to introduce the “brick-wall” model.¹ This model relies essentially on the idea that an interruption of the direct current path, i.e., a weak link or no connection at all between two platelike grains along their thin edges, can be bypassed if the supercurrent meanders through neighboring grains. The grain-to-grain connection is made by a partial overlap of the broad faces of two adjacent grains, i.e., generally by a twist grain boundary. Continuous refinements of the tape preparation process gave rise to highly improved tape performances. The microstructure of the high-current tapes, however, does not resemble a “brick wall” and the original brick-wall model¹ does not appropriately describe the current transport in high-quality tapes.

Detailed investigations performed on tapes with high critical-current densities j_c (*T* = 77 K, *B* = 0 T) > 15 kA/cm² led us to propose the “railway-switch” model³ with a more adequate microstructural foundation for high-quality tapes. The fundamental elements of our model are the small-angle *c*-axis tilt grain boundaries or “railway switches” that connect adjacent grains. They constitute those strong connections that are necessary to explain the observed high overall critical current densities. Furthermore there is evidence that the grain boundaries are not the dominant limiting factor for the critical-current density. The central objective of the present paper is to identify the mechanisms that limit the critical current in Bi/Pb (2223) silver-sheathed tapes.

The paper is organized as follows: In Sec. II we recapitulate the principles of the PIT process and give some basic information about the preparation of the samples used in this work. In Sec. III we present the main mi-

crostructural features of the Bi/Pb (2223) filament. In Sec. IV we review the central assumptions and implications of the railway-switch model. A comprehensive characterization of the electrical transport properties of the Bi/Pb (2223) silver-sheathed tapes has been performed in order to further refine the model and to allow reliable predictions of sample properties which in turn can be fed back into the preparation process. Measurements of the critical current parallel to the tape axis and normal to the tape plane will be presented in Secs. V and VI, respectively. We put the railway-switch model to a test by comparing a large set of transport current measurements to the model predictions. The spatial distribution of the critical current in the tapes is the topic of Sec. VII. We discuss the longitudinal critical-current distribution that can be derived from I - V characteristics and shortly address recent experimental results about the lateral critical-current distribution.⁴ Conclusions about the mechanisms that limit the critical-current density in the Bi/Pb (2223) silver-sheathed tapes will be drawn in Sec. VIII and starting points for a further improvement of the tape performance will be discussed. In the Appendix we analyze various definitions of the critical current and present some important experimental details and traps that should be avoided.

II. THE ESSENTIALS OF THE POWDER-IN-TUBE METHOD APPLIED TO $(\text{Bi, Pb})_2\text{Sr}_2\text{Ca}_2\text{Cu}_3\text{O}_{10}$ SILVER-SHEATHED TAPES

The standard powder-in-tube method is at first sight a very simple way to produce a composite conductor of considerable length, be it a wire or a tape. For the $(\text{Bi, Pb})_2\text{Sr}_2\text{Ca}_2\text{Cu}_3\text{O}_{10}$ tapes used in this work a silver tube is filled with a precursor powder for the final superconducting compound. Silver is used because of its high permeability for oxygen and its inert chemical behavior at the heat treatment temperatures ($T > 800^\circ\text{C}$). The precursor powder is essentially an oxide mixture that is obtained by prereacting a coprecipitated powder. The tube is sealed and subsequently deformed mechanically by swaging, drawing, and rolling to yield the desired form of the conductor which then consists of a powder filament inside a thin metal sheath. These green tapes are multiply heat treated with intermediate rolling which is necessary to compact the filament. The compaction step also improves the texture of the polycrystalline filament (a basic texture is already imposed by the cold-rolling process⁵ and is further enhanced by a reaction-induced texture that occurs during the first heat treatment⁶).

It should be noted that Bi/Pb (2223) cannot be obtained from a melt and that the solid-state reaction requires very long heat treatment times ($t > 100$ h). The presence of a small amount of a liquid phase that is formed in the course of the reaction from $\text{Bi}_2\text{Sr}_2\text{CaCu}_2\text{O}_8$ [Bi(2212)] to Bi/Pb(2223) is considered to be very important for obtaining high critical-current densities.

As final sample a monofilamentary tape of approximately three millimeters width and an overall thickness of roughly $100\ \mu\text{m}$ is obtained. The filament of superconducting Bi/Pb(2223) accounts for about one-third of the

total cross section [Fig. 1(a)]. The Bi/Pb(2223) grains are platelike and the typical texture of platelets in the filament can be seen in Fig. 2. In high-quality tapes only a small amount of secondary phases is present as remnants of an incomplete reaction of the precursor to the final Bi/Pb(2223) or a beginning decomposition of the just formed Bi/Pb(2223).

In the last years it became clear that some steps in the preparation procedure are more important than others in their possible limiting effects on the critical current, i.e., when the corresponding parameters are not perfectly adjusted. Most of these detrimental effects cannot be corrected in subsequent steps. The precursor powder, when contaminated with carbon (mainly from CO_2), sets an upper limit for the achievable critical-current density j_c .⁷ Strong variations of the filament thickness, "sausaging," can occur in the last rolling steps and degrade j_c as well as the mechanical properties of the tapes by introducing nominal points of fracture.⁸ Heat-treatment temperatures and times that are chosen to lie only slightly outside the very small optimum window (the temperature window has a width of only a few degrees) may lead to an incomplete reaction with a strong reduction of the critical current due to the detrimental influence of Bi(2212) at higher temperatures ($T > 70$ K). On the other hand a decomposition of the just formed Bi/Pb(2223) can occur when overshooting in temperature or time.

When speaking of optimizing the tape performance one should precisely define what optimum means, i.e., whether it correlates with the absolute value of j_c at $T = 77$ or 4.2 K, or with the respective magnetic-field dependences. The preparation parameters might be different for different performance criteria. An optimum $j_c(T = 77\ \text{K})$ does not necessarily mean that this is also true for $j_c(T = 4.2\ \text{K})$.

The samples that were investigated for this work were optimized in the sense that they were first of all prepared by a process that is industrially practicable and highly reproducible. This strict boundary condition excludes all

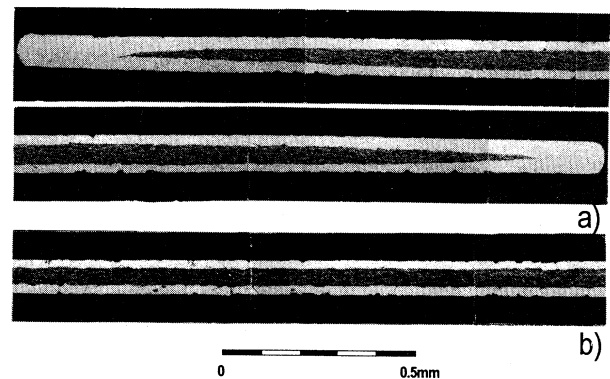


FIG. 1. Transverse (a) and longitudinal (b) cuts of a typical Bi/Pb (2223) tape with $j_c(T = 77\ \text{K}, B = 0\ \text{T}) = 24\ \text{kA/cm}^2$ [scanning electron microscopy (SEM); backscattered electrons; the Ag sheath appears in light gray colors, the Bi/Pb (2223) filament in dark gray]. The sample has been prepared by rolling as the only tape-forming process. The longitudinal cut has been taken in the middle of the filament.

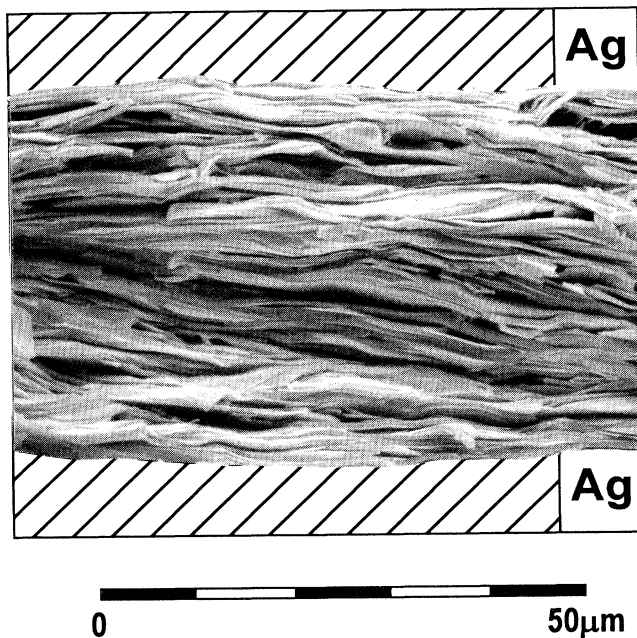


FIG. 2. Longitudinal fracture surface of the Bi/Pb (2223) filament of the same sample that is shown in Fig. 1 (SEM). The Ag sheath has been chemically removed prior to the fracture and the hatched regions mark the original position of the sheath. The fracture occurred in the middle of the filament.

process steps that can only be performed on short samples, e.g., uniaxial pressing. Besides this, as measure of sample quality the usual $j_c(T=77\text{ K}, B=0\text{ T}, 1\text{ }\mu\text{V/cm})$ was chosen. The cation ratio of the precursor powder was Bi:Pb:Sr:Ca:Cu = 1.72:0.34:1.83:1.97:3.13 and no further attempts have been made to optimize the stoichiometry with respect to j_c . More details of our standard preparation process can be found in Ref. 5. The critical-current densities of the tapes that have been prepared by rolling as the only tape forming process were $j_c(T=77\text{ K}, B=0\text{ T})=20\text{--}30\text{ kA/cm}^2$ throughout, with reproducibility in the sense that j_c is predictable, i.e., the critical-current density for samples prepared with a particular choice of parameters can be predicted within $\pm 2.5\text{ kA/cm}^2$. The values for the critical-current density of these "rolled-only" samples are not too far away from the highest ones published so far (January 1995, 38 kA/cm^2 , Ref. 9) and thus are representative for the state of the art in the field.

All features that are discussed in this work are typical features and have been reproducibly observed on all high-quality samples. Values that are given are typical average values, not typical best values and definitely not one-shot record values.

III. THE MICROSTRUCTURE OF SUPERCONDUCTING (Bi,Pb)₂Sr₂Ca₂Cu₃O₁₀ SILVER-SHEATHED TAPES

An illustration of the typical microstructure that is found in tapes with high critical-current densities is given in Figs. 2 and 3. The critical-current density at $T=77\text{ K}$ in self-field of the tapes shown in Figs. 2 and 3 was $j_c \approx 25$

kA/cm^2 . Figure 2 shows a longitudinal fracture surface that spans the whole thickness of the Bi/Pb (2223) filament. The main microstructural features, platelet size and alignment, do not differ significantly when comparing the layer near the Ag interface with the center of the filament. For early tapes with much lower j_c it has been observed that the platelets of the core were small and poorly textured, while the interface region near the silver consisted of longer and better aligned platelets. This led to the assumption that the current should preferentially flow in a thin layer near the Ag interface. A microstructure like the one shown in Fig. 2, however, indicates that this is probably not the case for optimized high-current tapes. We will show that the inhomogeneities on the scale of the thickness of the platelets (i.e., $\approx 1\text{ }\mu\text{m}$) dominate the transport properties, not those on the filament scale ($\approx 100\text{ }\mu\text{m}$), e.g., residual "sausaging." Figure 3

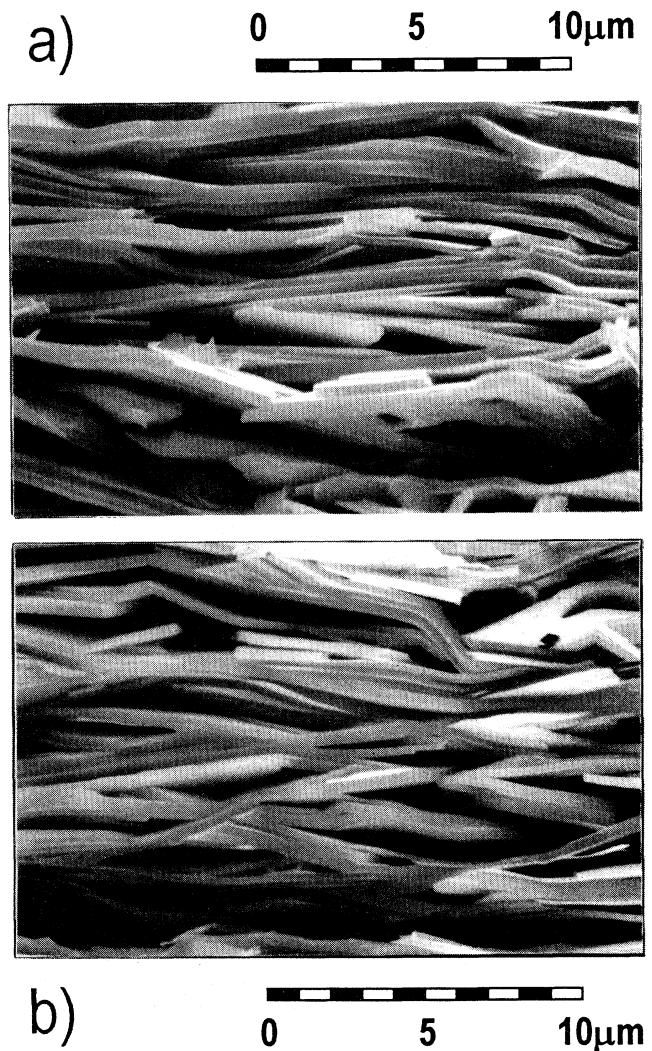


FIG. 3. Transverse (a) and longitudinal (b) fracture surfaces of a Bi/Pb (2223) filament with $j_c(T=77\text{ K}, B=0\text{ T})=25\text{ kA/cm}^2$ (SEM). The fractures were taken in the middle of the filament and span approximately half of the total filament thickness.

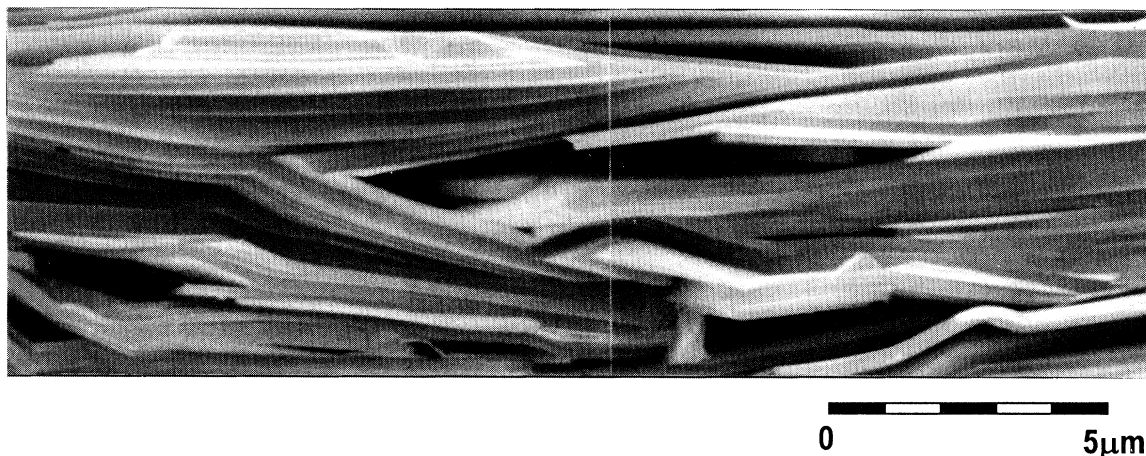


FIG. 4. A typical railway-switch network in a Bi/Pb (2223) filament (same tape as in Fig. 3; SEM).

compares a transverse (a) and a longitudinal (b) fracture surface of a Bi/Pb(2223) filament. The pictures extend over about half the total superconductor thickness. From the visual impression no significant differences between the microstructures in the longitudinal and transverse direction can be deduced.

In order to develop a model for the current transport one has to clearly identify the typical features of the microstructure. We will do this in two steps (i) the platelets that are visible in Figs. 2 and 3 and their internal structure have to be defined in their role for the current transport and (ii) the typical platelet-to-platelet connections together with the underlying grain-to-grain connections must be classified with respect to their transport properties and number density in the filament, thus giving an estimate of their overall importance.

A. Grains, colonies, and platelets

The platelets in Figs. 2 and 3 have a typical diameter of $D = 10\text{--}20\ \mu\text{m}$ and a thickness $d \approx 1\ \mu\text{m}$, thus aspect ra-

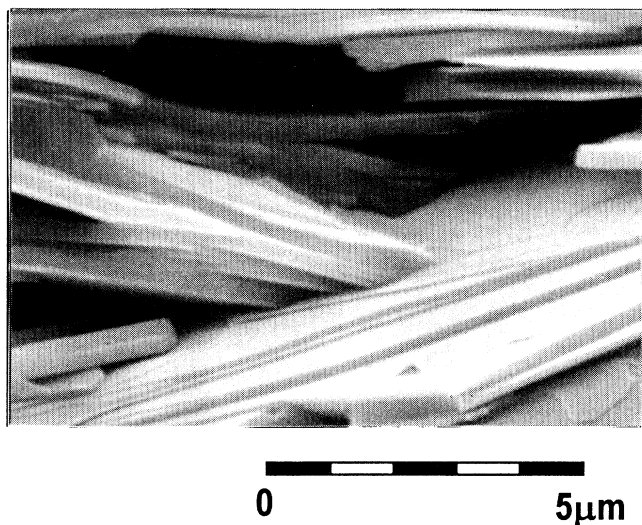


FIG. 5. Small-angle c -axis tilt (SCTILT) grain boundary connecting two Bi/Pb (2223) grains (SEM).

tios between 10 and 20. The substructure of the platelets that can already be deduced from Figs. 2 and 3 becomes more obvious in Figs. 4, 5, and 7. Each platelet is made up of a stack of grains ($d_{\text{grain}} \approx 100\ \text{nm}$; grain is used throughout this work in the sense of a single-crystalline unit). Numerous transmission electron microscopy (TEM) investigations^{10,11} revealed frequent (001) twist grain boundaries in Bi/Pb(2223). Two adjacent (Bi/Pb) 2223 layers have parallel c axes, while the a and b axes of the two layers can be more or less twisted around the common c axis. Several grains of (Bi/Pb)2223 with relative twist form a colony [Fig. 6(a)]. From the comparison with TEM results it is quite probable that the platelets observed in Figs. 2–5 and 7 are identical to these colonies. As scanning electron microscopy (SEM) does

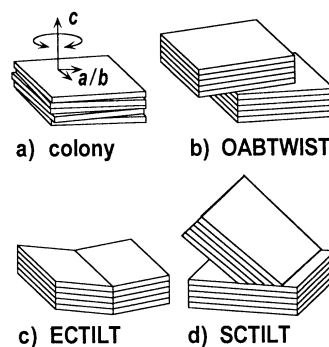


FIG. 6. Schematic representation of the dominant grain boundaries in the filament of high-current Bi/Pb (2223) silver-sheathed tapes. Each individual colony consists of a stack of grains with common c axis. Adjacent grains are separated by (001) twist boundaries (a). One type of colony boundary occurs by the partial overlap of the broad faces (or the a - b planes) of two adjacent colonies in a twist grain boundary (OABTWIST) (b). This type of colony boundary, however, is only rarely observed in the tapes. Edge-on c -axis tilt (ECTILT) grain boundaries (c) and small-angle c -axis tilt (SCTILT) grain boundaries (d) are the most frequently observed colony-to-colony connections. For simplicity the twist between the grains in the colonies is not shown in (b)–(d).

not reveal thin amorphous layers that eventually separate two colonies,¹¹ we will use the word “colony” in the just defined sense and platelet in its common meaning when referencing SEM pictures, e.g., Fig. 2.

The steps on the flat surface of the lower Bi/Pb(2223) platelet in Fig. 5 are the edges of the grains that form a colony. The grains preferentially grow along the *a-b* planes and practically no growth occurs along the *c* axis, in agreement with the experimental finding that the observed maximum thickness of the Bi/Pb(2223) platelets is limited to $d_{\max} \approx 2 \mu\text{m}$.

The colonies as the basic elements for the current transport are thus made up of stacks of grains with twist boundaries separating the grains (Figs. 5 and 7). The twist boundaries will generally reduce the critical-current density perpendicular to the *a-b* planes (depending on the twist angle)¹² and their effect can be described as an increase of the effective anisotropy of the critical current within the grain, i.e., the ratio of the in-plane critical-current density j_c^{ab} and the critical-current density j_c^c nor-

mal to the CuO_2 planes.

The crystalline perfection of the Bi/Pb(2223) grains will strongly influence their pinning properties. A perfect crystal without pinning-active defects will have a quite low critical-current density when the flux lines (or the stack of pancake vortices) are oriented perpendicular to the CuO_2 planes, i.e., parallel to the *c* axis. Just this, however, seems to be the case for the tapes and is plausible when one considers the long annealing times in proximity of the decomposition temperature of Bi/Pb(2223) that will certainly not promote the presence of crystallographic defects that could effectively pin magnetic-flux lines. Measurements of the critical-current density of the tapes indicate a relatively low pinning activity of the material when the magnetic field is oriented normal to the tape, i.e., nominally along the *c* axes of the grains. This is, however, an omnipresent feature of the Bi-based high-temperature superconductors (HTS) and thus not surprising. For the field direction with the flux lines oriented parallel to the CuO_2 layers on the other hand, the intrinsic plane pinning cannot take effect in the tapes as most grains are slightly misoriented and thus the majority of the grains experience a magnetic-field component in *c* direction at all orientations in the field. This fact will be discussed in Secs. V and VI.

Another characteristic feature of Bi-based HTS are mutual intergrowths of one or a few unit cells thickness, especially Bi(/Pb)(2212) in Bi/Pb(2223).¹³ All TEM investigations reveal, with varying frequency, the presence of Bi(/Pb)(2212) layers in Bi/Pb(2223) grains. Although the transformation process from Bi(2212) to Bi/Pb(2223) is not completely understood it is justified to assume that the Bi(/Pb)(2212) intergrowths are remnants of this particular process. The varying frequency of intergrowths that is reported can be explained by the fact that grains in different stages of the transformation have been investigated. The region near the Ag interface has been shown to transform first¹⁴ due to the promoting influence of the silver on the formation of the already mentioned liquid phase,¹⁵ thus they should have less intergrowths as they have been annealed longer than the grains in the central core of the filament. One important conclusion must be drawn from the observation of the intergrowths. If Bi/Pb(2223) grains with residual Bi(/Pb)(2212) layers are included in the path of the transport current and if the current flow along the *c* axis plays a significant limiting role, a qualitative change of the transport properties could occur at the critical temperature of the Bi(/Pb)2212 intergrowths¹⁶ (see Sec. V).

B. The classification of the grain boundaries

Little is known from direct experiments about the transport properties of individual Bi/Pb(2223) grains or colonies, not even to think of grain or colony boundaries. So far no high-quality Bi/Pb(2223) single crystals that would be suited for electrical measurements could be grown. This lack of knowledge is up to now bridged by transferring the results that have been obtained on Bi(2212) single crystals to Bi/Pb(2223). For the tapes, however, we can use an indirect approach to obtain more insight into the properties of the grain-to-grain (or

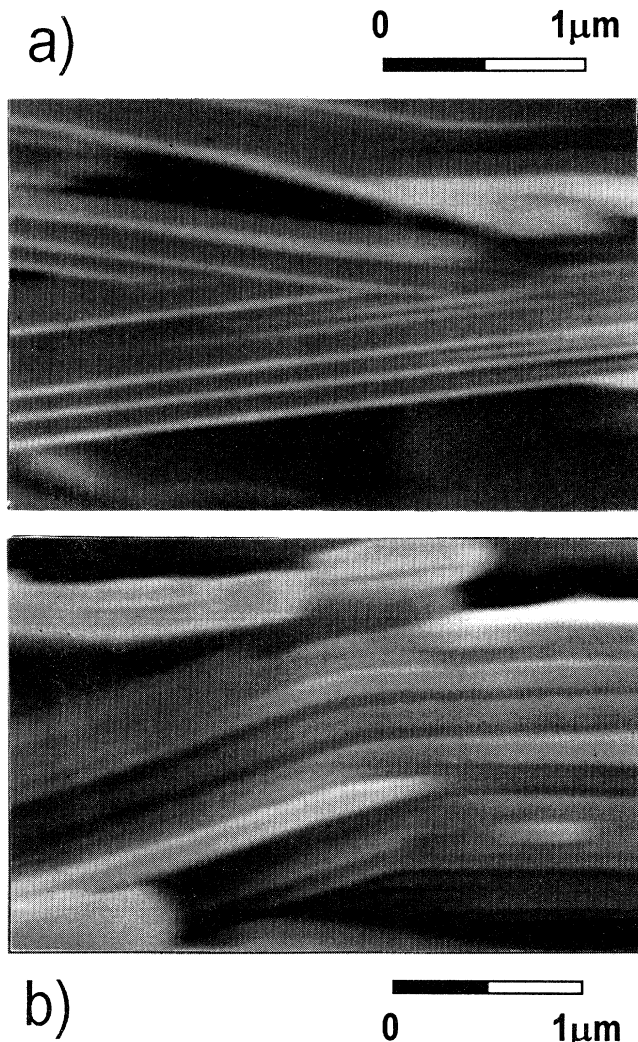


FIG. 7. Examples of SCTILT (a) and ECTILT (b) grain boundaries in Bi/Pb(2223) tapes (SEM). A series of ECTILT grain boundaries give the grains a softly bent or wavy shape (b).

colony-to-colony) connections.

The optimized tapes used in this work exhibit high critical-current densities $j_c(T=4.2\text{ K}, B=0\text{ T}) > 100\text{ kA/cm}^2$ and show a good performance in magnetic fields, without the typical signature of weak links for the transport current (see Sec. V). It must thus be possible to identify the strong electrical connections that are responsible for this fact. When speaking of electrical connections we will mainly address colony boundaries. One should, however, keep in mind that the individual grains in the colonies are already separated by twist grain boundaries and eventually also by phase intergrowths. Each particular colony boundary will then consist of several grain boundaries, eventually of different types.^{11,16} Being aware of this fact Fig. 6 schematically summarizes the three possible pure types of colony (grain) boundaries. A boundary that is formed by the partial overlap of the broad faces of two adjacent colonies is shown in Fig. 6(b) (OABTWIST). This type of boundary is evidently a twist grain boundary and forms the main building block of the brick-wall model. As can be verified by a closer look at Figs. 2–4 such colony boundaries are only rarely found in high-current Bi/Pb(2223) tapes. A second type of boundary is the edge-on c -axis tilt (ECTILT) boundary of Fig. 6(c). These ECTILT boundaries are formed by the touching edges of two neighboring colonies whose c axes lie in the same plane but are tilted with respect to each other. The ECTILT boundaries occur frequently and make the platelets look undulated (Figs. 2–5 and 7). The third type of boundary is the frequently observed small-angle c -axis tilt (SCTILT) boundary [Fig. 6(d)]. In the case of the SCTILT boundary the edge of one colony meets the broad face of another colony under a sharp angle. Figure 7 shows practical examples of ECTILT and SCTILT colony boundaries as seen by SEM.

As the current flows macroscopically through the tape it must also cross the frequent colony boundaries, ECTILT and SCTILT. In the following section we will discuss the possible limiting role of these colony boundaries for the supercurrent in the framework of the railway-switch model.

IV. THE RAILWAY-SWITCH MODEL

The first microstructural investigations of Bi/Pb(2223) silver-sheathed tapes that have been performed in the early days of development in the field revealed Bi/Pb(2223) platelets with a thickness $d \approx 1\text{ }\mu\text{m}$ (in the direction of the crystallographic c axis) and an average diameter $D \approx 10\text{ }\mu\text{m}$ (along the conducting CuO_2 layers in the a - b plane). The impression that the platelets in the filament were stacked like in a brick wall led Malozemoff² and Bulaevskii *et al.*¹ to coin the name “brick-wall” model for their description of the mechanisms of current transport in the tapes. The central idea of the brick-wall model^{1,17} (BWM) is that the current can overcome obstacles in the direct current path along the tape axis (i.e., fractures, weak links, and nonsuperconducting phases) by meandering around the interruptions through neighboring grains or colonies, thus crossing OABTWIST boundaries. The resulting winding current path of the BWM, but also any other current path in any other model obvi-

ously requires internal current flow along the c axis within individual grains or colonies, the necessary current density j_c^c depending on the aspect ratio. The anisotropy of the transport properties that is characteristic of high- T_c superconductors (HTS) manifests itself in a strongly reduced critical-current density j_c^c along the c axis as compared to the one along the a - b planes (j_c^{ab}). In the framework of the BWM this reduction must be compensated by the bigger cross section for the current in c direction as all current has to flow along the c axis. Up to now no values for j_c^c are available for Bi/Pb(2223) and data obtained for the structurally closely related Bi(2212) and $(\text{Bi,Pb})_2\text{Sr}_2\text{CaCu}_2\text{O}_8$ [Bi/Pb(2212)] remain the only source of information. Kleiner *et al.* found for single crystals of Bi(2212) that have been annealed in Ar that $j_c^c(4.2\text{ K}, B=0\text{ T}) \approx 150\text{ A/cm}^2$,¹⁸ while for Bi/Pb(2212) with up to 20% Pb for Bi and annealing in O_2/Ar considerably higher values up to $j_c^c(4.2\text{ K}, B=0\text{ T}) \approx 7\text{ kA/cm}^2$ have been measured.¹⁹ In both cases the layer-to-layer current was of Josephson nature, i.e., had weak-coupling character, and thus the crystals could be well described by a stack of Josephson junctions connected in series along the c axis. Wang *et al.* obtained $j_c^c(4.2\text{ K}, B=0\text{ T}) \approx 50\text{ A/cm}^2$ for the critical current across an OABTWIST grain boundary with a nominal twist angle $\theta_t=0^\circ$.¹² This “twist grain boundary” had been artificially prepared to obtain a reference value for j_c^c by resintering the two parts of a cleaved Bi(2212) crystal in their original orientation in 7.5% O_2/Ar . The restored nontwisted cleaving interface exhibited strong-coupling character, while for nonzero twist ($\theta_t=30^\circ, 36^\circ$) weak-coupling character has been observed.¹² The mentioned results are quite different but certainly can serve as estimates. For Bi/Pb(2212) j_c^c is by two orders of magnitude higher in agreement with the observation that the anisotropy in this compound is much smaller than in pure Bi(2212).²⁰ For the following we will assume that $j_c^c[\text{Bi/Pb}(2212)] \approx j_c^c[\text{Bi/Pb}(2223)]$, and as an order of magnitude for $j_c^c(4.2\text{ K}, B=0\text{ T}) \approx 5\text{ kA/cm}^2$ for Bi/Pb(2223).

After detailed scanning electron microscopy investigations of the microstructure of tapes with quite different overall critical-current densities we had to conclude that OABTWIST boundaries between two colonies are rare exceptions and that predominantly ECTILT and SCTILT boundaries connect neighboring colonies. Early high-resolution transmission electron microscopy analyses²¹ already revealed that the SCTILT boundaries are crystallographically very well defined and clean, even on an atomic scale. The wavy shape of the platelets in Figs. 2–4 results from a series of many ECTILT colony boundaries which are presumably annealed remnants of fractures that occurred in the course of the multiple mechanical deformations during the preparation process. Tapes with very low critical-current densities ($j_c < 10\text{ kA/cm}^2$ at 77 K in self-field) were found to contain small platelets with many free blunt edges and only few mutual connections. For tapes with higher critical-current densities [$j_c(77\text{ K}, B=0\text{ T}) > 10\text{ kA/cm}^2$] the morphology of the grains changes. The edges of the grains are sharp and

fewer free edges are observed, while the number density of ECTILT and SCTILT boundaries is strongly increased in comparison to low current tapes. An indication for the dominant role of these colony boundaries for the current transport is the fact that the normal-state resistivity along the tape axis is quite low [$\rho(150\text{ K}) \approx 500\ \mu\Omega\text{ cm}$] and its temperature dependence is found to be of pure a - b type,³ i.e., qualitatively identical to the in-plane resistivity of HTS thin films or single crystals. It can thus be concluded that the normal current in the filament is mainly flowing along the a - b planes and that in the normal state the current transport along the c axis does not contribute significantly to the resistivity (i.e., in the normal state there are either no OABTWIST boundaries incorporated in series in the current path or they are effectively shunted by ECTILT and SCTILT boundaries).

A polished longitudinal cross section of a Bi/Pb(2223) tape that looked like a track diagram of a train station led to the name “railway-switch” model after its fundamental elements, the small-angle c -axis tilt grain boundaries that play the role of railway switches. The railway-switch model (RSM)³ relies on the assumption that SCTILT boundaries constitute strong connections in the sense that they do not represent a weak link for the supercurrent with the detrimental effect of a strongly reduced critical current already in very small magnetic fields. An admittedly hypothetical but plausible argument for the strength of the connection might be the following: The characteristic length scale that determines the superconducting quality of a grain boundary is certainly given by the coherence length ξ . As has been shown for Bi(2212) the coherence length in c direction, ξ_c is too short as to enable strong connections even between the CuO_2 layers within one grain.^{18,19} The in-plane coherence length ξ_{ab} in turn is much longer and it seems more likely that a strong grain-to-grain connection can be achieved if ξ_{ab} is only long enough to penetrate the neighboring grain. For SCTILT and ECTILT boundaries this condition is certainly fulfilled and the strong links find their explanation.

The plausibility argument that has been given in the last paragraph seems to be in apparent contradiction with the results of Dimos, Chaudhari, and Mannhart²² on the superconducting transport properties of grain boundaries of HTS. These results were obtained on well defined grain boundaries in thin films that have been deposited on bicrystals with different relative orientation. Essentially all types of grain boundaries reduce the critical-current density by more than an order of magnitude when exceeding misorientation angles of about 10° . The ECTILT boundaries are very similar to the thin-film grain boundaries, while SCTILT boundaries cannot be realized in bicrystal experiments. In both cases, however, no substrate is present that could lead to additional distortions of the boundary. It should also be mentioned that the contact cross section of an SCTILT boundary grows like $1/\sin(\varphi)$ with decreasing tilt angle φ and is already enhanced by a factor of ≈ 4 for a 15° boundary and by ≈ 7 for 8° (relative to the constant transverse cross section of the grains). Thus the reduction of the critical-current density across the boundary is partly compensat-

ed for SCTILT boundaries. The railway-switch model is based on the assumption that neither ECTILT nor SCTILT boundaries are the dominant limiting elements in the current path. This fundamental assumption is supported by the fact that an improvement of the pinning properties of the grains by swift heavy ion irradiation leads to an enhancement of the critical current of the Bi/Pb (2223) tapes in magnetic fields.²³ This finding sharply contradicts a current limiting mechanism by grain boundaries.

In Fig. 8 we summarize the basic concepts of the railway-switch model. The involved current densities on the intragrain scale are j_c^{ab} and j_c^c along the a - b planes and along the c axis, respectively. The intracolony critical current density j_c^t across a twist grain boundary or across a Bi(/Pb)(2212) intergrowth is certainly lower than the intrinsic j_c^c . It is evident that the upper limit for the critical-current density from one broad face of a colony to the opposing face is given by the lowest j_c^t in the colony. The colonies eventually contain ECTILT boundaries that lead to an undulation of the platelets. Within the RSM the ECTILT boundaries modify the transport properties of the colonies, but they are not sufficient to explain the macroscopic current transport. The notion of “infinite” layers of grains along the tape direction that are connected by ECTILT boundaries is not sufficient to

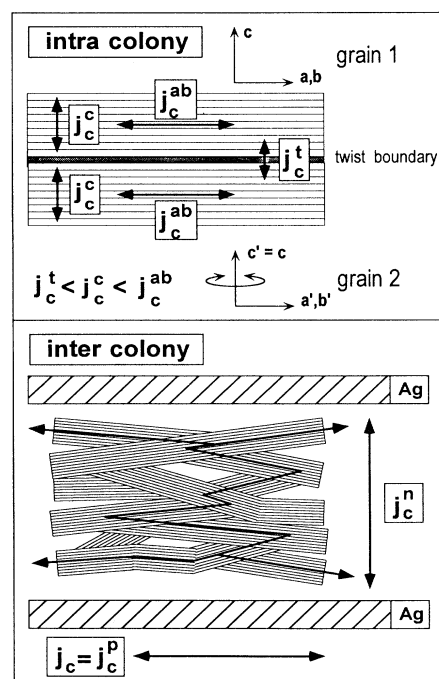


FIG. 8. Schematics of the microscopic (intracolony) and the macroscopic (intercolony) current flow in Bi/Pb (2223) silver-sheathed tapes. The involved critical-current densities are defined as follows: j_c^{ab} and j_c^c denote the intrinsic microscopic critical-current densities parallel to the a - b planes and along the c axis of Bi/Pb (2223) grains; j_c^t is the critical-current density across a twist boundary (i.e., between adjacent grains) or across a Bi(/Pb) (2212) intergrowth; the macroscopic critical-current densities parallel to the tape and normal to the tape are j_c and j_c^n , respectively. (Note: j_c^p is used synonymously to j_c .)

explain the observed high critical-current density j_c^n normal to the tape plane (see below under Sec. VI). The SCTILT boundaries are necessary for the formation of a $3d$ network, i.e., to connect the $2d$ layers that are internally connected by the ECTILT boundaries. The high j_c^n can only result from a $3d$ current path via SCTILT boundaries. The SCTILT boundaries are thus the important colony-to-colony connections. It should be noted that any macroscopic or intercolony current transport requires a microscopic current transfer from one face of the colony to the other (this is true for j_c and for j_c^n , the critical-current densities along the tape and normal to the tape plane, respectively). It is easy to verify that the average aspect ratio of the grains plays a key role for the macroscopic critical current.

V. THE CRITICAL-CURRENT DENSITY j_c PARALLEL TO THE TAPE

For this and the following sections the exact definition of the critical current is important. While different approaches to the problem are given in Appendix A we mention here only that in this section I_c denotes the critical current that has been determined by a voltage criterion of $1 \mu\text{V}/\text{cm}$. All derived quantities are thus based on this criterion. Considerably different absolute values are obtained by using different methods to determine I_c . They are, however, almost linearly correlated and thus relative or qualitative statements remain practically unaffected by the choice of the method.

A. The temperature dependence of the critical-current density $j_c(T)$ parallel to the tape

The typical temperature dependence of the critical-current density along the tape axis, $j_c(T)$, is shown in Fig. 9. Besides the zero-field curve, measurements in various external magnetic fields B are shown for a field orientation parallel to the broad face of the tape ($\theta=90^\circ$; θ is the angle between the tape normal and the magnetic field; the magnetic field is oriented perpendicular to the current). A linear variation of j_c with temperature is ob-

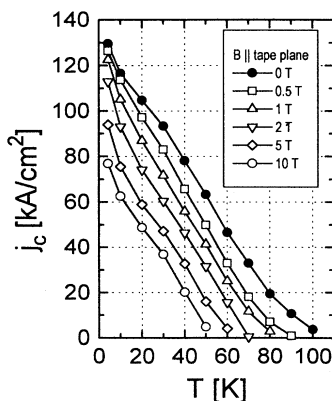


FIG. 9. Temperature dependence of the critical-current density of a Bi/Pb (2223) silver-sheathed tape. For the measurements in different applied magnetic fields (open symbols) the field was oriented parallel to the tape plane and perpendicular to the current.

served. The effect of the external magnetic field is a shift of the curves in the direction of the origin without qualitative changes of the temperature dependence (this is also true for $\theta=0^\circ$, i.e., when the magnetic field is oriented normal to the tape plane). Many earlier samples showed a quite distinct change of slope in $j_c(T, B=0 \text{ T})$ near 80 K. We had attributed this effect to either untransformed Bi/(Pb)(2212) grains in parts of the current path or to Bi/(Pb)(2212) intergrowths in the Bi/Pb(2223) grains.²⁴ Optimized samples like the one of Fig. 9 do not show such a distinct change of slope but a continuously decreasing slope, i.e., a foot at temperatures above $T=80 \text{ K}$.

From measurements of $j_c(T)$ alone, no conclusion can be drawn whether Bi/(Pb)(2212) is incorporated in the Bi/Pb(2223) current path or not. However, it cannot be excluded that Bi/(Pb)(2212) intergrowths are even present in the grains of high-current tapes, although with strongly reduced frequency, as they are found in practically all grains of Bi/Pb(2223).^{10,11} It should be mentioned that intergrowths are not the only imaginable origin of a change of slope or a curvature of $j_c(T)$ near T_c and that further investigations are necessary to elucidate the role of the intergrowths for the critical current by correlating their presence and number density (as visualized by TEM) with the transport properties of the tapes (like it has already been started in Ref. 16).

Besides these considerations it can be stated that the temperature dependence $j_c(T)$ (without and with external magnetic field) of Bi/Pb(2223) tapes with $j_c(T=77 \text{ K}, B=0 \text{ T}) > 20 \text{ kA}/\text{cm}^2$ resembles the one that is characteristic for high-quality thin HTS films and gives no hints for the presence of weak links in the current path. This does, of course, not mean that no weak links could be found somewhere in the samples as the transport measurements test only the best parts of the sample and with different experimental methods one might test also the parts that do not contribute to the critical transport current.

B. The magnetic field dependence of the critical-current density $j_c(B, T)$ parallel to the tape

The question whether or not the critical transport current in the tapes is limited by weak links can be clarified by analyzing the field dependence $j_c(B)$. Weak links lead to a strong decrease of j_c in magnetic fields but a strong decrease alone does not necessarily mean that weak links must be involved. It has been shown by Bulavskii *et al.* that the field dependence of the critical current, including the initial drop at low fields can be remarkably well described when the imperfect texture is taken into account.¹⁷ A lack of pinning due to high crystalline perfection with only few pinning centers together with an imperfect texture might delude the observer into believing in weak links where in reality there are none. Our interpretation of $j_c(B, T)$ relies on just these assumptions and does not need any weak links in the current path, except the unavoidable intrinsic ones along the c axis.

A complication arises by irreversibilities in the field dependence $j_c(B)$ that occur at low temperatures and due

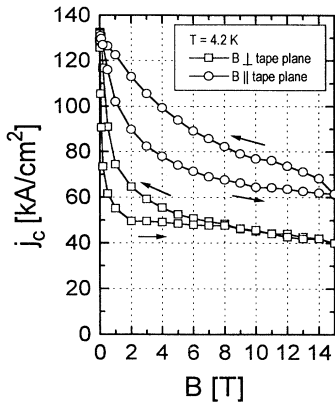


FIG. 10. Hysteresis of the critical transport-current density of a Bi/Pb (2223) tape at 4.2 K for two field orientations (the magnetic field was oriented parallel or normal to the tape plane; $B \perp j$).

to which $j_c(B)$ becomes dependent on the measurement history of the sample. Figure 10 demonstrates the hysteretic behavior of $j_c(B)$ in increasing and decreasing fields at 4.2 K for two field orientations (the magnetic field B is oriented normal, $\theta=0^\circ$, or parallel, $\theta=90^\circ$, to the tape plane; $B \perp j$). In both cases the sample had been exposed to a magnetic field $B=15$ T and only then the curves for increasing and subsequently for decreasing field have been measured. The observed strong hysteresis decreases with increasing temperature. The origin of the irreversible behavior of $j_c(B)$ is not yet completely clear and a more detailed discussion of this interesting effect will be given elsewhere.⁵ In connection with the present work mainly the curves obtained in decreasing field will be considered.

Figure 11 shows the field dependences $j_c(B)$ at temperatures between $T=4.2$ and 100 K for both mentioned sample orientations in the magnetic field. Both sets of data are qualitatively similar, but differ by a factor of 5 to 10 in field. We extrapolate the decay to $j_c(B) \rightarrow 0$ and thus define the critical field B_{c2}^{jc} , i.e., the magnetic field at which j_c vanishes at a certain temperature. The obtained temperature dependences $B_{c2}^{jc}(T)$ are shown in Fig. 12 (the results for increasing field are identical). As the ex-

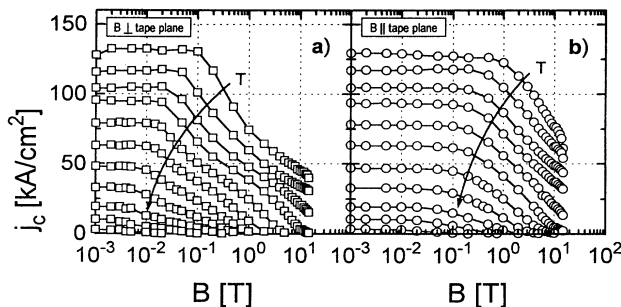


FIG. 11. Magnetic-field dependence of the critical-current density of a Bi/Pb (2223) tape for two field orientations [normal (a) and parallel (b) to the tape plane; $B \perp j$] at various temperatures $T=4.2, 10, 20, 30, 40, 50, 60, 70, 80, 90,$ and 100 K; the direction of increasing temperature is indicated by the arrows.

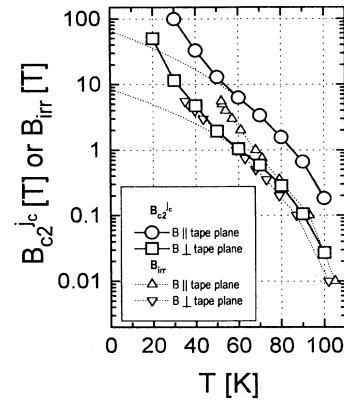


FIG. 12. Temperature dependence of the critical magnetic field B_{c2}^{jc} of a Bi/Pb(2223) tape determined from transport measurements (for the definition of B_{c2}^{jc} see text). The magnetic field was oriented normal or parallel to the tape plane ($B \perp j$). The corresponding irreversibility lines B_{irr} for a similar sample have been obtained by magnetic measurements (data for B_{irr} from Ref. 25). The dotted lines extrapolate the high-temperature behavior to temperatures below the inflection point at $T=50$ K.

trapolation becomes very ambiguous no values for B_{c2}^{jc} are given for temperatures below $T=20$ K. An inflection of $B_{c2}^{jc}(T)$ is observed around $T=50$ K. Extrapolating the high-temperature behavior (dotted lines) to temperatures below the inflection point it can be stated that below $T=50$ K an overproportional increase in the critical field occurs and thus also in the critical current.

The critical field B_{c2}^{jc} can be identified with the irreversibility field B_{irr} that is obtained from magnetic measurements. The magnetic irreversibility lines $B_{irr}(T)$ for the two field orientations that have been measured on a tape similar to the ones used for this work²⁵ are also shown in Fig. 12. A good agreement of $B_{c2}^{jc}(T)$ with $B_{irr}(T)$ is observed when the field is applied normal to the tape plane, while for the other orientation the two curves are found to be quite different. This might find its explanation in the fact that for $B_{c2}^{jc}(T, \theta=0^\circ)$, $B_{c2}^{jc}(T, \theta=90^\circ)$, and $B_{irr}(T, \theta=0^\circ)$ the transport current as well as the magnetically induced current flow within the tape plane, while for $B_{irr}(T, \theta=90^\circ)$ a current perpendicular to the tape plane is necessary to shield the external magnetic field. The magnetic irreversibility field $B_{irr}(T, \theta=90^\circ)$ that is significantly reduced in comparison to $B_{c2}^{jc}(T, \theta=90^\circ)$ suggests that the lower critical-current density perpendicular to the tape plane is not compensated by the bigger cross section and thus limits the critical-current density that is obtained by this type of measurement.

For the anisotropy of the critical field $\beta(T) = B_{c2}^{jc}(T, \theta=90^\circ) / B_{c2}^{jc}(T, \theta=0^\circ)$ an almost constant value of $\beta \approx 6$ is found from 100 down to 60 K. At lower temperatures $\beta(T)$ increases slightly with decreasing temperature. From high-field measurements it is known that $\beta < 2$ at 4.2 K, implying a maximum of the anisotropy $\beta(T)$ of the critical field somewhere between 10 and 20 K. The very similar shape of the $B_{c2}^{jc}(T)$ curves for the two

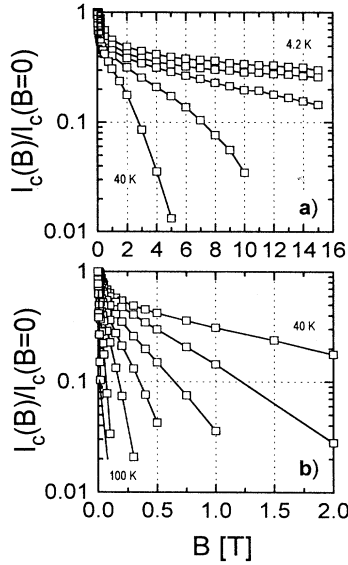


FIG. 13. Normalized magnetic-field dependence of the critical current of a high-current Bi/Pb (2223) tape in a field normal to the tape plane ($B \perp j$). (a) $T = 4.2, 10, 20, 30,$ and 40 K; (b) $T = 40, 50, 60, 70, 80, 90,$ and 100 K.

field orientations suggests that they have the same origin. This strong correlation is in fact predicted by the railway-switch model.

At temperatures above $T \approx 50$ K the critical current decays exponentially with magnetic field for both tape orientations in the field, i.e., $j_c/j_{c0} = \exp(-B/B_0)$, with deviations from this behavior in very low fields only, as can be seen in Figs. 13(b) and 14(b). The characteristic field $B_0(\theta=90^\circ)$ is a factor of 5 to 10 higher than $B_0(\theta=0^\circ)$. At lower temperatures ($T < 50$ K) a qualita-

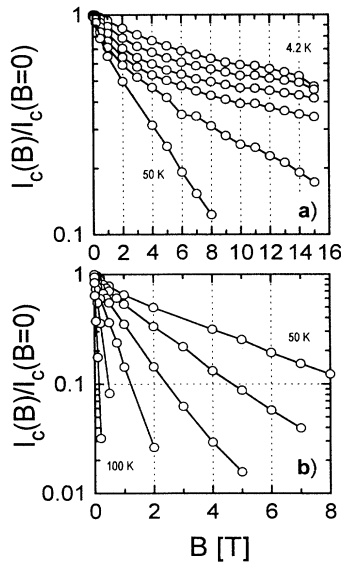


FIG. 14. Normalized magnetic-field dependence of the critical current of a high-current Bi/Pb (2223) tape in a field parallel to the tape plane ($B \parallel j$). (a) $T = 4.2, 10, 20, 30, 40,$ and 50 K; (b) $T = 50, 60, 70, 80, 90,$ and 100 K.

tive change of $I_c(B)$ is observed [Figs. 13(a) and 14(a)]. The detrimental effect of the magnetic field on the critical current is strongly reduced below $T = 50$ K and high values of j_c are sustained even in high fields ($B > 10$ T) resulting in a high B_{c2}^j as already mentioned. The observed behavior of $I_c(B, \theta=0^\circ)$ is typical for Bi-based HTS when the field is applied parallel to the c axis. Bi/Pb(2223) tapes qualitatively show the same field dependence that is known from high quality Bi/Pb(2223) films²⁶ or from epitaxial films or single crystals of Bi(2212) at the same reduced temperature $t = T/T_c$.

The question arises whether a change in the pinning mechanism is responsible for the qualitative change of $j_c(B)$ at lower temperatures, i.e., below the inflection point at $T \approx 50$ K. An answer is found by analyzing the pinning-force density $f_p = B j_c$ and its scaling function $\mathcal{F}(B/B_{c2}^j)$. In many cases the pinning-force density can be well described by $f_p = f_{p,0} [B_{c2}^j(T)]^m \mathcal{F}(b)$,²⁷ with B_{c2}^j being the critical magnetic field at which f_p vanishes, $b = B/B_{c2}^j$, the reduced magnetic field and $f_{p,0}$ a constant. The scaling function is $\mathcal{F}(b) = b^p(1-b)^q$. In Fig. 15(a) the normalized pinning-force density f_p/f_p^{\max} for $20 \text{ K} \leq T \leq 100 \text{ K}$ is shown (with the magnetic field oriented normal to the tape surface, $\theta=0^\circ$; $B \perp j$). From independent fits of all curves the critical magnetic field B_{c2}^j , the maximum pinning force density f_p^{\max} and values for $p \approx 1$ and $q \approx 4$ are found. Within experimental error all curves can be well described by $\mathcal{F}(b) = b(1-b)^4$, simi-

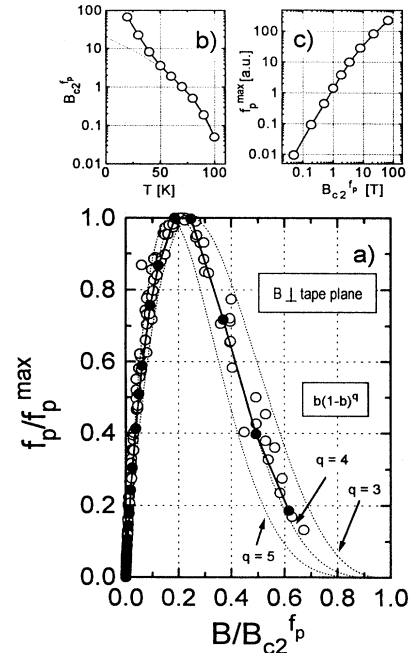


FIG. 15. Normalized volume pinning force f_p/f_p^{\max} of a Bi/Pb (2223) tape as a function of the reduced magnetic field $b = B/B_{c2}^j$ normal to the tape plane (B_{c2}^j is defined in the text; $B \perp j$) (a). The solid symbols represent the data at $T = 40$ K. The open symbols represent all other data for $T = 20, 30, 50, 60, 70, 80, 90,$ and 100 K. The critical magnetic field B_{c2}^j as a function of temperature is shown in (b), while the maximum volume pinning force as a function of B_{c2}^j is shown in (c).

lar to Bi(2212) single crystals.²⁸ Data for $T < 20$ K have not been considered as f_p does not reach its maximum f_p^{\max} at the maximum available field $B \leq 15$ T and thus the fits become very ambiguous. In Fig. 15(b) the obtained $B_{c2}^{f_p}(T, \theta=0^\circ)$ is shown and not surprisingly the same features are present that have been found for $B_{c2}^{j_c}(T, \theta=0^\circ)$, i.e., an inflection point around $T=50$ K. The parameter m can be estimated from Fig. 15(c) to $m \approx 2$ at high temperatures and $m < 2$ for $T < 50$ K, again comparable to results obtained for Bi(2212) single crystals.²⁸ If we assume that the pinning mechanism is described only by the scaling function $\mathcal{F}(b)$ it must be concluded from the above results that the pinning mechanism does not change from T_c down to 20 K (and possibly even to 4.2 K), but that mainly a strong increase of the critical magnetic field $B_{c2}^{f_p}(T, \theta=0^\circ)$ at low temperatures leads to the observed high critical currents in magnetic fields.

There is strong evidence that the Bi/Pb(2223) grains are very well connected and behave like one big elongated grain. At low temperatures $T < 50$ K a high critical-current density is sustained in magnetic fields of considerable strength. The high sensitivity to magnetic fields parallel to the c axis at high temperatures results from the lack of effective pinning centers as it is the case for high-quality HTS films and single crystals.

VI. THE CRITICAL-CURRENT DENSITY j_c^n NORMAL TO THE TAPE

The determination of the critical current I_c^n normal to the tape plane by a simple voltage criterion involves several difficulties, mainly because of the extremely short current path perpendicular to the tape ($l \approx 40 \mu\text{m}$). For a quantitative comparison with the critical current I_c along the tape axis a criterion independent quantity, the most probable critical current I_c^{\max} is derived from the I - V curves (see Appendix A for its definition). The measurement of the critical current I_c^n normal to the tape is in general not an easy task and requires the careful consideration of many experimental details in order to avoid misinterpretation of the results. In Appendix B we present our experimental setup together with some basic conceptual ideas.

A. The field dependence and the anisotropy of the critical-current density $j_c^n(\theta, B, T=77 \text{ K})$ normal to the tape in external magnetic fields

The field dependence of the critical-current density normal to the tape, j_c^n puts any model for the current transport to a severe test. In the framework of the railway-switch model³ the current path for j_c^n consists of a zigzag route from one side of the filament to the other. A direct way via OABTWIST grain boundaries is predicted by the brick-wall model,^{1,17} but is not realized, as can be seen from the microstructures in Figs. 2–4. However, both models, railway-switch and brick-wall have in common that the very same mechanism of current transport must work in the two different experimental setups (j_c and j_c^n) and that thus the magnetic-field dependences $j_c(B)$ and $j_c^n(B)$ should be identical. The same distinction

between the models that is made for j_c is also valid for j_c^n . The net supercurrent flows along the a - b planes and is transferred to the neighboring platelets via “railway-switches” without current along their c axes (railway-switch model) or directly across an OABTWIST boundary along the c axis (brick-wall model).

Figure 16(a) shows the normalized field dependence $I_c^n(B)/I_c^n(B=0)$ at $T=77$ K and for comparison the corresponding $I_c(B)/I_c(B=0)$. When the field is applied parallel to the tape plane both magnetic-field dependences [$I_c(B, \theta=90^\circ)$, $I_c^n(B, \theta=90^\circ)$] are almost identical. For a magnetic field normal to the tape plane, however, a distinctly different behavior is found. $I_c(B, \theta=0^\circ)$ shows the typical strong reduction of the critical current already in low fields, while $I_c^n(B, \theta=0^\circ)$ is much less affected by the magnetic field. If a lack of flux pinning is made responsible for the high sensitivity of I_c to magnetic fields it must be concluded that for $I_c^n(B, \theta=0^\circ)$ the flux lines are kept from moving or less force is applied, as j_c^n decreases less with B . The setup for $I_c^n(B, \theta=0^\circ)$ is in fact the force-free configuration in which the flux lines are aligned with the current direction. It should be mentioned that at first sight only the nominal direction of the current is directed perpendicular to the tape plane. As a first approximation the RSM assumes that the current should mainly flow along the a - b planes of the colonies and be transferred to other colonies via railway switches. Thus the flux lines would not be force free and the finding that $I_c^n(B)/I_c^n(B=0) \neq I_c(B)/I_c(B=0)$ (for $B \perp \text{tape}$) seems to be in apparent contradiction to the RSM. This is, however, not the case, as the current has also to be transferred from one side of a colony to the other and it is just this intracolony current that is dominant in the experimental setup for I_c^n .

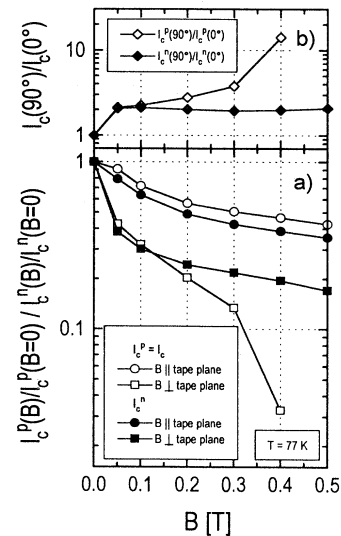


FIG. 16. Normalized magnetic-field dependence of the critical currents parallel to the tape plane, $I_c^p = I_c$, and normal to the tape plane I_c^n for the two field orientations parallel and normal to the tape plane at $T=77$ K (a). I_c^p and I_c^n are defined as the most probable critical currents (see Appendix A for its definition). The corresponding anisotropy ratios $I_c(90^\circ)/I_c(0^\circ)$ for the two cases, I_c^p and I_c^n , are also shown (b).

The measured critical-current densities that correspond to the normalization values $I_c(T=77\text{ K}, B=0\text{ T})$ and $I_c^n(T=77\text{ K}, B=0\text{ T})$ of Fig. 15 are $j_c \approx 25\text{ kA/cm}^2$ and $j_c^n \approx 2.5\text{ kA/cm}^2$. Thus for the tapes the anisotropy of the critical transport-current density at $T=77\text{ K}$ is $j_c/j_c^n \approx 10$ and in both cases the currents are qualitatively a - b currents. The last statement had already been confirmed by Cho in Ref. 29.

In small magnetic fields the same mechanisms seem to determine j_c and j_c^n . This becomes clear from the angular dependence of the critical-current density in a small external magnetic field. Figure 17 shows $I_c^n(\theta)/I_c^n(\theta=90^\circ)$ and $I_c(\theta)/I_c(\theta=90^\circ)$ for $B=0.1\text{ T}$ and $T=77\text{ K}$. The curves for both current directions are identical and show that I_c as well as I_c^n depend only on the magnetic-field component normal to the tape, i.e., nominally parallel to the c axes of the grains.

B. The current-transfer length L_{ct}

The critical current perpendicular to the tape plane does not only bear an academic interest within the RSM but is technologically very important as it determines the current-transfer length L_{ct} , i.e., the length along the tape direction over which the current is distributed over the whole sample cross section. In normal experimental setups the current is fed into the tape on one of the broad faces and it is assumed that the high conductivity of the silver sheath promotes a short-scale current transfer to the filament. This assumption is certainly fulfilled, as generally no effects of the sample length are observed, even for very short samples ($l < 1\text{ cm}$). In order to avoid the contribution of the sheath we used a “sandwich” configuration to determine L_{ct} of the filament alone. For this purpose the long edges of a tape were cut in order to avoid any direct contact between the two opposing silver sheaths. On the so prepared sample, a sandwich of Ag/Bi,Pb (2223)/Ag, contacts for current and voltage were attached from both sides. The total sample length was only $l \approx 10\text{ mm}$ with contact spacings of $d = 1\text{ mm}$

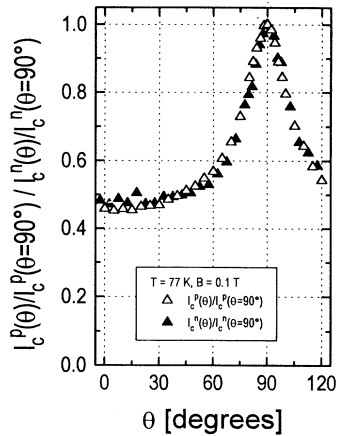


FIG. 17. Normalized angular dependences of the critical current $I_c(\theta)/I_c(\theta=90^\circ)$ for the two critical currents parallel (I_c^p) and normal (I_c^n) to the tape plane at $T=77\text{ K}$ and $B=0.1\text{ T}$. The critical current is defined as the most probable critical current I_c^{\max} (see Appendix A for its definition).

(for all further details see Appendix B).

I - V curves have been measured in two contact configurations: (i) “same side,” i.e., current and voltage contacts on the same side of the sample (ss), and (ii) “opposite side,” i.e., the voltage contacts were on the opposite side of the current contacts (os). In order to eliminate small geometrical variations two measurements were made in both cases, by using the same configuration but interchanging the sides. For the following we assume that the voltage drop across the voltage taps is proportional to the current that flows in the silver sheath to which the contacts are attached.

We find that in the normal state at room temperature only about one third of the voltage that is produced on the same side appears on the opposite side. It should be mentioned that the sandwich setup is considerably different from the “transformer” setup that has been used to determine the c -axis resistivity ρ_c of Bi(2212) crystals.³⁰ The “sandwich” is more appropriate for critical-current measurements when the sample is superconducting, while the transformer setup is well suited for resistivity measurements when the sample is normal conducting. Being aware of the involved uncertainties an estimated value for the resistivity perpendicular to the tape plane at room temperature $\rho^n \approx 5\text{ m}\Omega\text{ cm}$ can nevertheless be obtained. This low value is an indication that the current flows predominantly along the a - b planes, in a zigzag current path that is probably 10 to 20 times longer than the filament thickness.

Figure 18 shows the normalized field dependences ($\theta=0^\circ, 90^\circ; B \perp j$) of the critical current $I_c(B)/I_c(B=0\text{ T})$ at $T=77\text{ K}$ for the (ss) and the (os) configuration. I_c has either been determined by a voltage criterion [$1\mu\text{V/cm}$; Fig. 18(a)] or by the maximum of the longitudinal critical-current distribution $p(I_c)$ [I_c^{\max} , see next section and Appendix A for its definition; Fig. 18(b)]. Only the data for one set of measurements are shown as the results

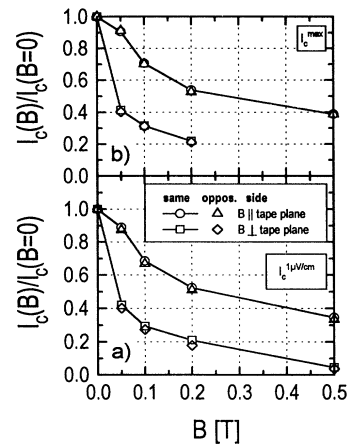


FIG. 18. Normalized field dependence of the critical current in “sandwich configuration” (for details of the experiment see text and Appendix B). Within experimental resolution the same critical current in “same-side” and “opposite-side” configuration is obtained for both field orientations and both used I_c criteria. A criterion of $1\mu\text{V/cm}$ was applied in (a), while in (b) the most probable critical current I_c^{\max} was used (see Appendix A for its definition).

are identical for interchanged sides. The sandwich experiment shows that the current-transfer length in optimized monofilamentary tapes with $j_c > 20 \text{ kA/cm}^2$ is certainly $L_{ct} < 2 \text{ mm}$, or probably even less (the contact spacing between the current and the voltage taps was 2 mm). This finding has an important implication for the technique of joining two tapes, as it is very probable that high current-carrying superconducting joints can be achieved over relatively short lengths.

Considering the low critical-current density j_c^c along the c axis it must be concluded that the short current-transfer length L_{ct} and the underlying relatively high critical-current density j_c^n normal to the tape plane can only result from a zigzag current path and not from a direct path.

VII. THE SPATIAL DISTRIBUTION OF THE CRITICAL CURRENT

The spatial critical-current distribution in the filament has been a matter of controversy since the first Bi,Pb(2223) tapes have been prepared. It has been widely assumed that the current flows mainly in a thin layer of longer, highly aligned platelets near the silver interface. Other studies were devoted to the question of the transverse³¹ and longitudinal³² distributions of the critical current. We will present transverse and longitudinal distributions for the high-quality tapes that have been used throughout this work. These distributions have been obtained reproducibly and are characteristic for our tapes with $j_c(T=77 \text{ K}, B=0 \text{ T}) > 20 \text{ kA/cm}^2$.

The association of a “sharp” I - V curve with a homogeneous sample and a smooth and more gradual transition with inhomogeneities in the superconducting current path can be described quantitatively as follows: assuming a longitudinal distribution $p(I_c)$ of the local critical-current density I_c one finds that the second derivative of the I - V curve qualitatively describes the critical-current distribution by $d^2V/dI^2 = \text{const } p(I_c)$.^{33,34} These considerations are of course only valid if the intrinsic resistive transition is well defined and not already excessively broadened.

In case of the silver-sheathed Bi,Pb(2223) tapes two main sources of longitudinal inhomogeneity can be distinguished. A locally different I_c along the tape axis occurs due to a variation of the cross section of the filament, i.e., mainly of the thickness. This “sausaging” is caused by the rolling process. The second origin for a varying critical current are inhomogeneities in the filament itself that can mainly be attributed to a different number density of electrically strong connections (“railway switches”) or to different amounts of secondary phases.

Although the rolling process that was used for the preparation of the tapes for this work has been carefully optimized it was not possible to eliminate the sausaging completely. A residual sausaging is always caused by rolling due to the softness of the silver sheath in comparison with the hard ceramic core. A typical example of a longitudinal cross section of a filament is shown in Fig. 19 [see also Fig. 1(b)]. By a quantitative analysis of the residual

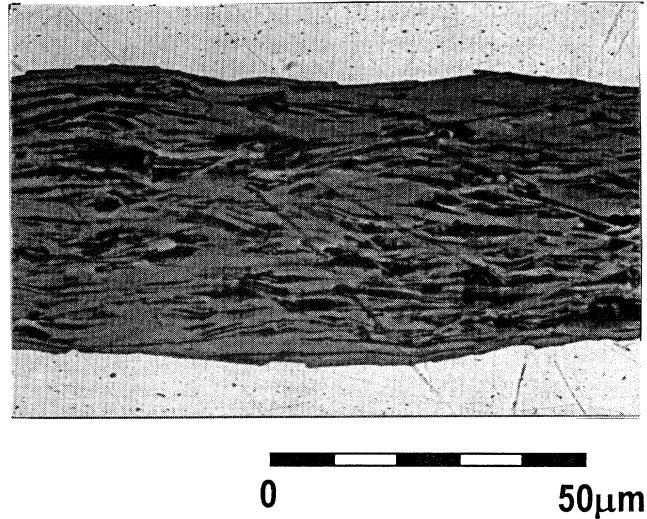


FIG. 19. Polished cross section of the central part of a rolled Bi/Pb (2223) silver-sheathed tape (SEM; backscattered electrons; see also Fig. 1). For the analysis of the residual sausaging the thickness of the filament has been measured in the middle of the filament over a total distance of 5 mm at intervals of $10 \mu\text{m}$.

sausaging it is, however, possible to separate it from other inhomogeneities in the filament. The analysis is based on the statistical evaluation of measurements of the local thickness of the filament. Typically the thickness is measured in the middle of the filament at distances $d = 10 \mu\text{m}$ over a total length $l = 5 \text{ mm}$. The result of the analysis is shown in Fig. 20 for a green tape (a), a rolled tape after final reaction (b) and for comparison also for a pressed tape in the final state (c). The distribution of the thickness variation has Gaussian form and indicates that many random factors must be playing a role. No difference is found between the distributions for the green tape and the rolled tape. This is an indication that the “sausaging” is caused by the cold mechanical deformation process and remains unchanged over the subsequent heat treatments. The uniaxial pressing results in a broader distribution and indicates that the pressure is not distributed homogeneously over the sample (although the distribution and thus also the critical current is generally

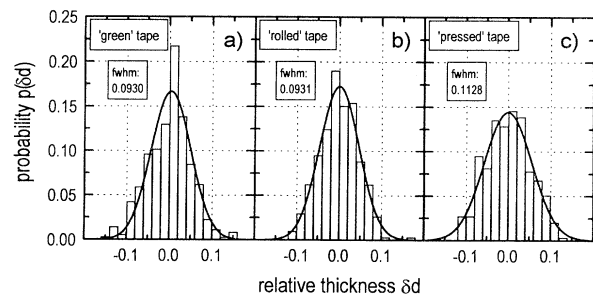


FIG. 20. Normalized probability distribution of the relative filament thickness of a tape after cold rolling before the heat treatment [green tape (a)], after the final heat treatment [rolled tape (b)] and for comparison for a multiply pressed tape after the final heat treatment [pressed tape (c)].

shifted to higher currents uniaxial pressing is not applicable for the production of long lengths of tapes). The residual sausing of the rolled tapes [Fig. 20(b)] that have been investigated for this work is given by the full width at half maximum of the thickness distribution and amounts to roughly 10%.

Figure 21 shows a typical I - V curve (a) and its first (b) and second (c) derivative. The main problem in obtaining $p(I_c) \propto d^2V/dI^2$ is the uncontrollable self-heating of the sample. Even when contact resistances are not taken into account there is still a considerable amount of power that is dissipated in the sample [Fig. 21(b)]. It is easily understandable that the associated self-heating will strongly increase when in most parts of the sample the critical current is exceeded. In other words self-heating effects become important at currents above the most probable critical current I_c^{\max} . The expected Gaussian distribution $p(I_c)$ is disturbed by self-heating above I_c^{\max} , while on the low current side a perfect distribution is observed [Fig. 21(c)]. For the following we will determine I_c^{\max} and the width of the distribution by fitting a Gaussian profile only to the undisturbed low-current half (for details see Appendix A).

A comparison of the thickness distribution (Fig. 20) and the critical-current distribution [Fig. 21(c)] is shown in Fig. 22. The widths of the distributions differ by almost a factor of 3. This clearly proves that the residual "sausaging" is not the only origin for the longitudinal variations of the critical current. To a bigger part microscopic inhomogeneities of the filament must be responsible for the broadening of the I - V curve. It is worthwhile noting that all attempts to fit physical laws to I - V curves of Bi,Pb(2223) tapes make absolutely no sense if the influence of all these inhomogeneities is not taken into account (even before attempting a fit, the silver contribution must of course be subtracted).

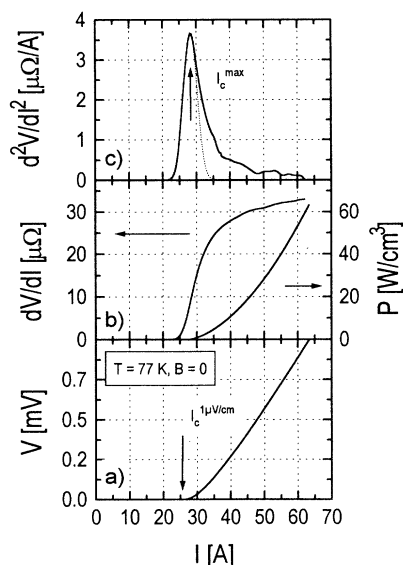


FIG. 21. Typical I - V curve for a rolled Bi/Pb (2223) tape at $T = 77$ K and $B = 0$ T (a). First (b) and second (c) derivative of the same I - V curve in (b) the dissipated power density as a function of the applied current is also shown.

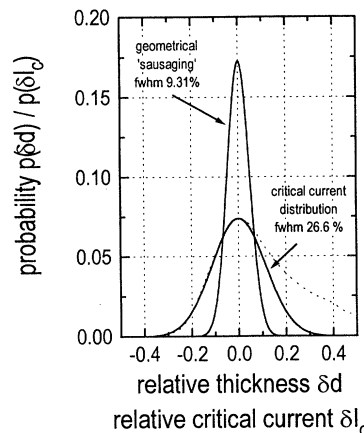


FIG. 22. Comparison of the macroscopic sausing as given by the thickness distribution of the filament (geometrical sausing) and the microscopic "sausaging" as determined by the longitudinal critical-current distribution that is obtained from the second derivative of the I - V curve.

If the microscopic inhomogeneities were of mere geometrical nature they should lead to a temperature and field independent width of the distribution. In Fig. 23(b) the temperature dependence of the width of the critical-current distribution is shown. The width increases with temperature between 4.2 and 90 K by only 50%. It is thus very probable that most of the inhomogeneities are in fact geometrical, i.e., the effective cross section varies locally.

The inhomogeneities that we discussed above are a series of "bottlenecks." There is, however, also the possibility that the critical current is nonhomogeneously distributed over the filament cross section. While this is cer-

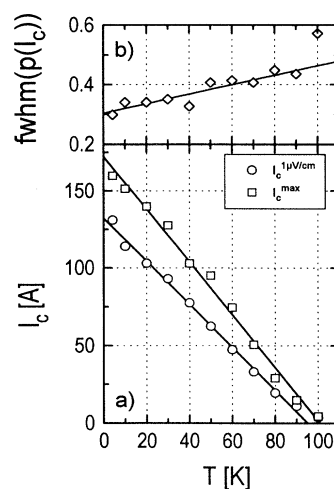


FIG. 23. Temperature dependence of the critical current for two criteria ($1 \mu\text{V}/\text{cm}$ and I_c^{\max} , see Appendix A for details). Over the whole temperature range the results obtained by both criteria are qualitatively identical except for a multiplicative factor (a). Variation of the width of the longitudinal critical-current distribution $p(I_c)$ with temperature (b).

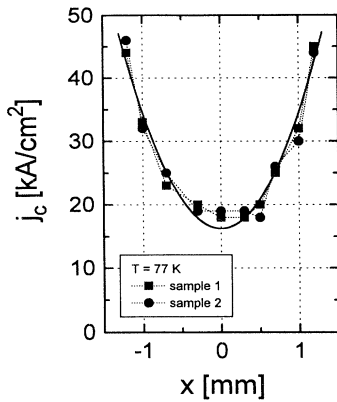


FIG. 24. Distribution of the critical-current density along the width of two rolled Bi/Pb (2223) silver-sheathed tapes (Data from Ref. 4). The critical-current density $j_c(x)$ at $T=77$ K systematically varies by almost a factor of 3 and reaches its highest values ($j_c \approx 50$ kA/cm²) at the long edges where the filament is thinnest. The solid line represents a parabolic dependence.

tainly true on a microscopic scale we have to address the question whether there is also a systematic distribution on a macroscopic scale. For this purpose we have directly measured the lateral critical current distribution $j_c(x)$ along the width of the tape.⁴

Attempts to directly measure $j_c(x)$ have been performed by Larbalestier *et al.*³¹ They cut thin longitudinal strips from a tape and measured the critical current of the individual strips. These experiments provided the evidence for a nonhomogeneous critical-current density distribution $j_c(x)$ for the Bi₁Pb(2223) tapes. Our method also consists in cutting thin longitudinal strips from a tape but then the critical current of the remaining rest of the tape is measured and not of the cut strip.⁴

It can be seen from Fig. 24 that for two typical tapes with an overall $j_c(T=77$ K, $B=0$ T) ≈ 23 kA/cm² the local critical-current density varies by a factor of 2–3 and that the critical-current density is strongly enhanced at the thin edges of the tape. The distribution is symmetric and has been reproducibly obtained for several samples. Possible origins for the distribution $j_c(x)$ are discussed in Ref. 4.

VIII. CONCLUSIONS

The microstructure of Bi₁Pb(2223) silver-sheathed tapes with critical-current densities $j_c(77$ K, $B=0$ T) > 20 kA/cm² does not resemble the dense regular structure of a brick wall. The majority of colony-to-colony connections (colony=stack of grains with (001) twist boundaries separating them) is made by small-angle c -axis tilt boundaries and not by partial overlapping of the a - b planes in twist boundaries. This statement implies that the brick-wall model^{1,17} that assumes a quite different microstructure is not applicable to high-current Bi₁Pb(2223) tapes. The railway-switch model³ is microstructurally more appropriate and much closer to the real conditions in the description of the colony-to-colony

current transport. One of the central statements of the railway-switch model is that the critical transport current along the tape is not limited by grain-boundary weak links. The notion of the tape being a “big grain” with peculiar internal properties (as compared to a real single crystal) describes the situation quite adequately and is widely confirmed by data of the transport properties. The answer to the question what limits the critical-current density has been found in the grain (or better the colony) itself, independent of the model for the colony-to-colony current transport.

Only recently reliable data became available that threw light on the mechanism of the current transport along the c axis of Bi-based HTS. It turns out that the extreme structural anisotropy, although being extremely helpful in creating highly textured microstructures is in fact also the main limitation for the critical-current density. The low critical-current density j_c^c perpendicular to the CuO₂ planes compared to the in-plane critical-current density j_c^{ab} does not promote a distribution of the supercurrent in the individual grains, especially in grains with a small aspect ratio. On the level of the colony the problem is even aggravated by an increase of the effective anisotropy of the critical current due to twist boundaries and intergrowths. All this leads to an inefficient use of the available cross section for the current, or in other words many possible “channels” for the current are not used and they are often separated from the main current path by “barriers” in the form of twist boundaries or intergrowths. A peculiar consequence of this fact is that transport measurements do not reveal this scenario directly. All respective data indicate that there are no special bottlenecks, e.g., weak links, but the measured critical-current density remains inexplicably low. This is because the transport current is only sensitive to serial bottlenecks and not to parallel ones.

The major limitation by j_c^c determines an upper limit for the achievable critical-current density. The other parameter that determines this limit besides j_c^c is the average aspect ratio of the grains and colonies. Longer grains and colonies certainly increase the current-carrying capacity of the tapes. Just this has been one of the reasons for the positive development of the tape performance over the last years. Starting from the “envelope” that is given by j_c^c and the aspect ratio other mechanisms further reduce the critical current in magnetic fields. Effective pinning centers can be introduced by heavy ion irradiation,²³ while the texture, as well as the spatial homogeneity can be further improved by more and more sophisticated preparation processes, but all this can only relieve the secondary level of limitation, not the primary one. Within the framework of the railway-switch model a perfect texture would result in a strongly reduced critical current, as a currently still undetermined optimum tilt angle $\phi_{opt} \neq 0^\circ$ exists for the railway switches ($0^\circ < \phi_{opt} < 10^\circ$).

It will be a major breakthrough when it will be possible to reduce the intrinsic anisotropy by refined metallurgic treatments. This requires, however, a considerable change in the way of thinking. The potential of the material itself is by far not used to full advantage.

ACKNOWLEDGMENTS

The authors are grateful to A. Jeremie, A. Perin, and J.-C. Grivel for numerous helpful discussions and an always stimulating atmosphere. We thank M. R. Cimberle for the permission to use some data prior to publication. This work has been supported by the Swiss National Science Foundation (PNR30), the Swiss Priority Program "Materials Research and Engineering" (PPM), and the European Community (Brite Euram II).

APPENDIX A

The definition of the critical current generally makes use of a voltage criterion, the most common being $1 \mu\text{V}/\text{cm}$. Although this method is quite arbitrary it is widely used because of its convenience. The next more realistic step is to include the sample cross section in the determination and to extend the voltage criterion to a resistivity criterion, e.g., $10^{-14} \Omega\text{m}$. Although already much more physical this method must also rely on an arbitrarily defined threshold value. For sharp transitions that are typical for high-quality samples of conventional superconductors at low temperatures the choice of a criterion was not critical, as it changed the result only insignificantly. The situation, however, is different for HTS with broad transitions at high temperatures and in magnetic fields.

Figure 25(a) shows a log-log plot of a typical I - V curve of a Bi,Pb(2223) silver-sheathed tape at 77 K. The measured voltage range extends over more than seven orders of magnitude. The curvature at higher voltages results from the part of the current that flows through the silver sheath. This contribution can be subtracted by assuming that at a voltage V a current $I_s = V/R_s$ flows through the silver sheath (R_s is the resistance of the sheath). The I - V curve can then be corrected by subtracting I_s from the total current. Unfortunately it is practically impossible to precisely determine R_s (even in high magnetic fields, where the superconducting contribution of the filament is assumed to be more or less suppressed). Because of this ambiguity we did not try to correct our I - V curves. This correction is generally also not necessary as the curves differ significantly only at voltages $V > 20 \mu\text{V}$, i.e., far above the $1 \mu\text{V}/\text{cm}$ criterion for short samples.

On the basis of high-quality data it is possible to extrapolate the I - V curve to a criterion of $0 \mu\text{V}/\text{cm}$, or in other words to eliminate the criterion. The necessary assumption is that the curve can be described by $V \propto (I - I_c)^\alpha$. For conventional superconductors it has been widely assumed that $V \propto I^n$.³⁵ The resistive transition index n , or shorter n factor is a measure for the homogeneity of the sample. High transition indices $n > 50$ were found for high-quality Nb-Ti wires.³⁴ Recently the correlation between the width of a Gaussian critical-current distribution and the n factor has been demonstrated by Edelman and Larbalestier.³² From Fig. 25 it is, however, evident that the simple relation $V \propto I^n$ does not hold for the tapes and must be replaced by $V \propto (I - I_c)^\alpha$ [the nonlinearity of the I - V curve in the log-

log plot and thus the deviation from $V \propto I^n$ is obvious from the continuous variation of $d(\log V)/d(\log I)$ in Fig. 25(b)]. A best fit to $V \propto (I - I_c)^\alpha$ (only data below $10 \mu\text{V}$) can be obtained with $I_c = 9.7 \text{ A}$ and $\alpha = 8.2$. The curve that is obtained after subtraction of the criterion independent critical current $I_c = 9.7 \text{ A}$ is also shown in Fig. 25(a). It should be mentioned that due to the residual sausing and to the microscopic inhomogeneities (see Sec. VII) no higher α 's can be expected for the Bi,Pb(2223) tapes. Preliminary results indicate that the refined resistive transition index α is widely temperature and field independent and closely related to the width of the distribution $p(I_c)$ of the critical current. A detailed discussion of this finding will be given elsewhere.³⁶

Another criterion independent critical current can be obtained from the second derivative of the I - V curve by determining the current at which the maximum in the critical-current distribution (i.e., d^2V/dI^2) occurs. This current is the most probable critical current I_c^{max} . Most probable means that I_c^{max} is the value of the critical current that is locally most frequently found in the sample (longitudinally).

Figure 21(c) shows d^2V/dI^2 for the critical current I_c along the tape axis, while Fig. 26(c) shows the same for I_c^{max} along the tape normal. It can be seen from Fig. 26(a) that a simple voltage criterion would result in very different

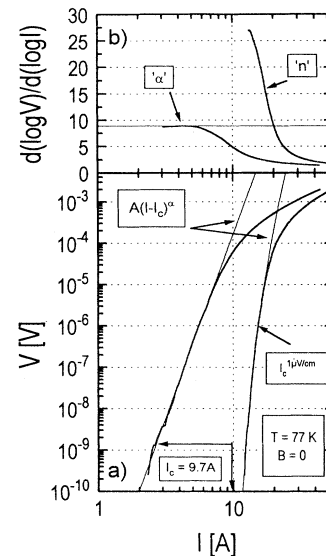


FIG. 25. Typical I - V curve of a rolled Bi/Pb (2223) tape in log-log representation (a). Besides the standard $1 \mu\text{V}/\text{cm}$ criterion a fit of the I - V curve with $V = A(I - I_c)^\alpha$ is shown ($A = \text{const}$). The new I - V curve is then obtained by subtracting I_c that has been found by the fit. The logarithmic derivative $d(\log V)/d(\log I)$ of the two curves in (a) is shown in (b). While the slope of the original curve (i.e., the commonly used n factor or resistive transition index) constantly varies over the whole range, α remains essentially constant and thus is independent of the voltage at which the slope is determined (the voltage range above $10 \mu\text{V}$ is not considered here because of the curvature that results from the part of the current that passes through the silver sheath).

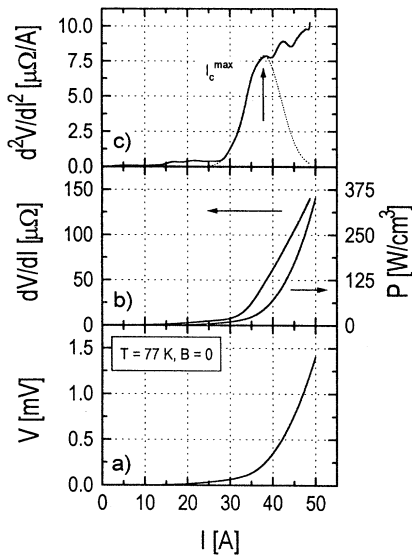


FIG. 26. Typical I - V curve for a current perpendicular to the broad face of a Bi/Pb (2223) tape. Spurious voltages appear due to the unavoidable imperfect four-probe measurement (i.e., a small residual voltage drop occurs across the top and bottom Ag sheaths that serve as voltage taps, but are electrically too well connected with the superconducting filament). A criterion, like $1 \mu\text{V}/\text{cm}$ is thus not applicable. Like in Fig. 21 the first (b) and second (c) derivatives are also shown. The self-heating effects in this case are more pronounced, as is evident from the higher dissipated power density (b) in the absence of a stabilization by a silver shunt (top and bottom sheath are completely separated).

values for I_c^n ("low current foot" due to contact resistances; see under B below) and that the heating effects are even more important in this case as the stabilizing silver sheath has been taken away for this experiment. Under the realistic assumption that the width of the distribution d^2V/dI^2 is mainly due to geometrical inhomogeneities a linear correlation between I_c^{max} and $I_c^{1\mu\text{V}/\text{cm}}$ is obtained [see Fig. 23(a)].

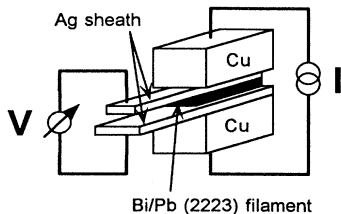


FIG. 27. Experimental setup for the measurement of the critical current I_c^n normal to the tape plane. For this type of experiment it must be assured that no direct silver-silver connection exists between the top and bottom sheaths. The effects of self-heating must be carefully considered as the involved currents and dissipated power densities are relatively high.

APPENDIX B

Some preliminary considerations are necessary before attempting to measure the critical-current density along the tape normal I_c^n . As the geometry is far from being suited for a classical four-probe setup it is necessary to eliminate most of the disturbing contact resistances and to increase the sample resistance as much as possible. The latter can be achieved by removing any electrical contact between the two halves of the silver sheath on the broad faces of the tape (this is an absolute must) and by reducing the sample cross section to the useful minimum (typically $1\text{--}2 \text{ mm}^2$). The remaining silver foils might seem to provide low contact resistances and help to distribute the current homogeneously over the sample cross section. This is only true at first sight and turns even to the opposite when we imagine that the whole setup represents a series connection of a resistance (silver), a perfect conductor [Bi,Pb(2223)] and again a resistance (silver). Through this configuration the current will possibly find a very tortuous way and thus attaching separate current and voltage contacts to the silver will result in completely unrepresentative results (this is not a hypothesis but has been verified experimentally). In our setup we use copper blocks as current contacts and the two silver sheaths as voltage contacts (Fig. 27). It can be easily understood that this is the configuration that is nearest to classical four probe, although a very small residual contact resistance cannot be eliminated.

Figure 28 shows the setup for the "sandwich" experiment. The upper and lower contact assemblies consist of

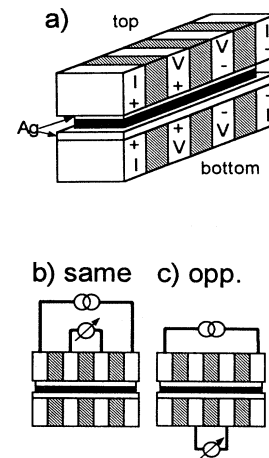


FIG. 28. The "sandwich" experiment. Stacks of alternatingly isolating and conducting layers are attached as top and bottom electrodes to a tape with completely separated top and bottom sheaths (a). The voltage can be measured on the side of the current contacts ["same side" configuration (b)] or on the opposite side ["opposite side" configuration (c)]. In order to eliminate geometrical differences the measurements are performed twice with exchanged sides.

alternating Cu and insulating layers. As the two sets of contacts are pressed onto the sample it has been verified that the pressure does not create any damage in the sample. For this purpose the sample has been measured in

another rig before and after the measurement in the "sandwich." No differences of the critical current have been found after using both types of sample holder (Fig. 27 and Fig. 28).

*On leave from Consorzio INFM, Università di Genova, Genova, Italy.

- ¹L. N. Bulaevskii, J. R. Clem, L. I. Glazman, and A. P. Malozemoff, *Phys. Rev. B* **45**, 2545 (1992).
- ²A. P. Malozemoff, in *Superconductivity and its Applications*, edited by Y. H. Kao, A. E. Kaloyeros, and H. S. Kwok, AIP Conf. Proc. No. 251 (AIP, New York, 1992), p. 6.
- ³B. Hensel, J.-C. Grivel, A. Jeremie, A. Perin, A. Pollini, and R. Flükiger, *Physica C* **205**, 329 (1993).
- ⁴G. Grasso, B. Hensel, A. Jeremie, and R. Flükiger, *Physica C* **241**, 45 (1994).
- ⁵G. Grasso (unpublished).
- ⁶N. Merchant, J. S. Luo, V. A. Maroni, G. N. Riley, Jr., and W. L. Carter, *Appl. Phys. Lett.* **65**, 1039 (1994).
- ⁷A. Jeremie, R. Flükiger, and E. W. Seibt, *IEEE Trans. Magn.* **30**, 1883 (1994).
- ⁸K. Osamura, M. Kamo, S. S. Oh, and S. Ochiai, *Cryogenics* **34**, 303 (1994).
- ⁹T. Hikata, K. Muranaka, S. Kobayashi, J. Fujikami, M. Ueyama, T. Kato, T. Kaneko, H. Mukai, K. Ohkura, N. Shibuta, and K. Sato (unpublished).
- ¹⁰A. Umezawa, Y. Feng, H. S. Edelman, D. C. Larbalestier, Y. S. Sung, E. E. Hellstrom, and S. Fleshler, *Physica C* **198**, 261 (1992).
- ¹¹H. K. Liu, R. K. Wang, and S. X. Dou, *Physica C* **229**, 39 (1994).
- ¹²Jyh-Lih Wang, X. Y. Cai, R. J. Kelley, M. D. Vaudin, S. E. Babcock, and D. C. Larbalestier, *Physica C* **230**, 189 (1994).
- ¹³L. Ranno, D. Martínez-García, J. Perrière, and P. Barboux, *Phys. Rev. B* **48**, 13 945 (1993).
- ¹⁴Yi Feng, Y. E. High, D. C. Larbalestier, Y. S. Sung, and E. E. Hellstrom, *Appl. Phys. Lett.* **62**, 1553 (1993).
- ¹⁵J.-C. Grivel and R. Flükiger, *Physica C* **229**, 177 (1994).
- ¹⁶A. Umezawa, Y. Feng, H. S. Edelman, T. C. Willis, J. A. Parrell, D. C. Larbalestier, G. N. Riley, Jr., and W. L. Carter, *Physica C* **219**, 378 (1994).
- ¹⁷L. N. Bulaevskii, L. L. Daemen, M. P. Maley, and J. Y. Coulter, *Phys. Rev. B* **48**, 13 798 (1993).
- ¹⁸R. Kleiner, P. Müller, H. Kohlstedt, N. F. Pedersen, and S. Sakai, *Phys. Rev. B* **50**, 3942 (1994).
- ¹⁹R. Kleiner and P. Müller, *Phys. Rev. B* **49**, 1327 (1994).
- ²⁰F. X. Régi, J. Schneck, H. Savary, C. Daguet, and F. Huet, *IEEE Trans. Appl. Supercond.* **3**, 1190 (1993).
- ²¹T. Hikata, H. Mukai, K. Sato, and H. Hitotsuyanagi, *Sumitomo Elect. Tech. Rev.* **29**, 45 (1990).
- ²²D. Dimos, P. Chaudhari, and J. Mannhart, *Phys. Rev. B* **41**, 4038 (1990).
- ²³P. Kummeth, C. Struller, H.-W. Neumüller, and G. Saemann-Ischenko, *Appl. Phys. Lett.* **65**, 1302 (1994).
- ²⁴B. Hensel, G. Grasso, A. Perin, and R. Flükiger, in *TMS Conference Proceedings of the Symposium on Processing of Long Lengths of Superconductors, Pittsburgh '93*, edited by U. Balachandran *et al.* (The Minerals, Metals & Materials Society, Warrendale, PA, 1994), p. 269.
- ²⁵V. Calzona, M. R. Cimberle, C. Ferdeghini, R. Flükiger, G. Grasso, D. Marré, M. Putti, C. Rizzuto, and A. S. Siri, *Proceedings of the 15th ICEC*, Genoa, Italy, 1994 [*Cryogenics* **34**, 801 (1994)].
- ²⁶H. Yamasaki, K. Endo, S. Kosaka, M. Umeda, S. Misawa, S. Yoshida, and K. Kajimura, *IEEE Trans. Appl. Supercond.* **3**, 1536 (1993).
- ²⁷A. M. Campbell and J. E. Evetts, *Critical Currents in Superconductors* (Taylor and Francis, London, 1972).
- ²⁸M. Mittag, M. Rosenberg, D. Peligrad, R. Wernhardt, V. A. M. Brabers, J. H. P. M. Emmen, and D. Hu, *Supercond. Sci. Technol.* **7**, 214 (1994).
- ²⁹J. H. Cho, M. P. Maley, J. O. Willis, J. Y. Coulter, L. N. Bulaevskii, P. Haldar, and L. R. Motowidlo, *Appl. Phys. Lett.* **64**, 3030 (1994).
- ³⁰R. Busch, G. Ries, H. Werthner, G. Kreselmeyer, and G. Saemann-Ischenko, *Phys. Rev. Lett.* **69**, 522 (1992).
- ³¹D. C. Larbalestier, X. Y. Cai, Y. Feng, H. Edelman, A. Umezawa, G. N. Riley, and W. L. Carter, *Physica C* **221**, 299 (1994).
- ³²H. S. Edelman and D. C. Larbalestier, *J. Appl. Phys.* **74**, 3312 (1993).
- ³³J. Baixeras and G. Fournet, *J. Phys. Chem. Solids* **28**, 1541 (1967).
- ³⁴W. H. Warnes and D. C. Larbalestier, *Cryogenics* **26**, 643 (1986).
- ³⁵F. Volker, *Part. Accel.* **1**, 205 (1970).
- ³⁶B. Hensel (unpublished).

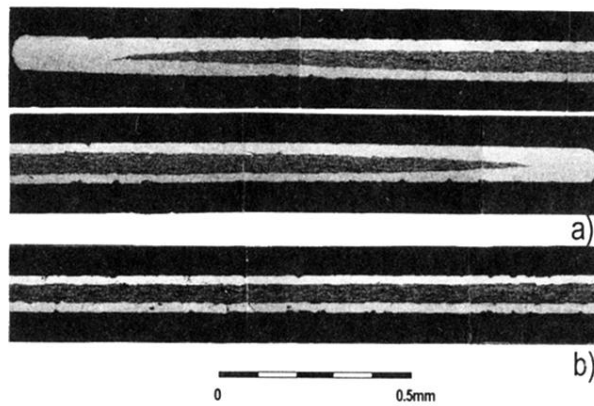
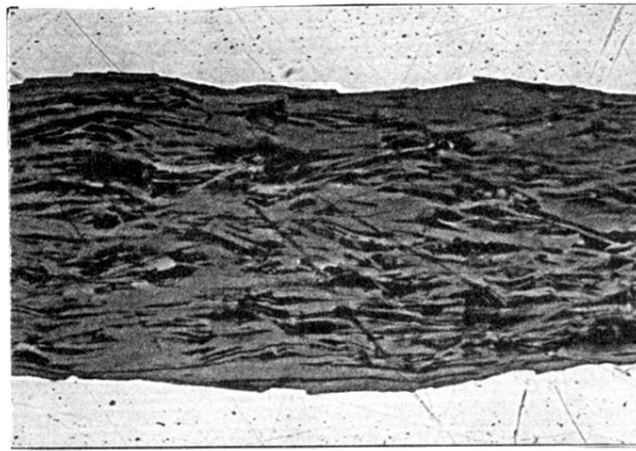


FIG. 1. Transverse (a) and longitudinal (b) cuts of a typical Bi/Pb (2223) tape with $j_c(T=77\text{ K}, B=0\text{ T})=24\text{ kA/cm}^2$ [scanning electron microscopy (SEM); backscattered electrons; the Ag sheath appears in light gray colors, the Bi/Pb (2223) filament in dark gray]. The sample has been prepared by rolling as the only tape-forming process. The longitudinal cut has been taken in the middle of the filament.



0 50 μ m

FIG. 19. Polished cross section of the central part of a rolled Bi/Pb (2223) silver-sheathed tape (SEM; backscattered electrons; see also Fig. 1). For the analysis of the residual sausaging the thickness of the filament has been measured in the middle of the filament over a total distance of 5 mm at intervals of 10 μ m.

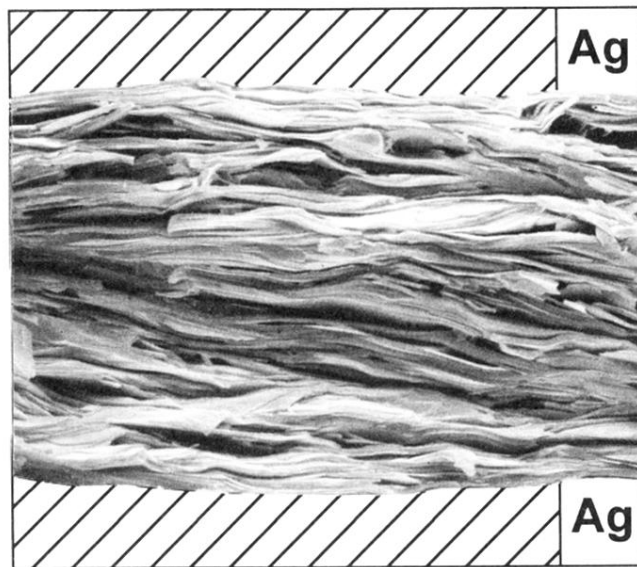


FIG. 2. Longitudinal fracture surface of the Bi/Pb (2223) filament of the same sample that is shown in Fig. 1 (SEM). The Ag sheath has been chemically removed prior to the fracture and the hatched regions mark the original position of the sheath. The fracture occurred in the middle of the filament.

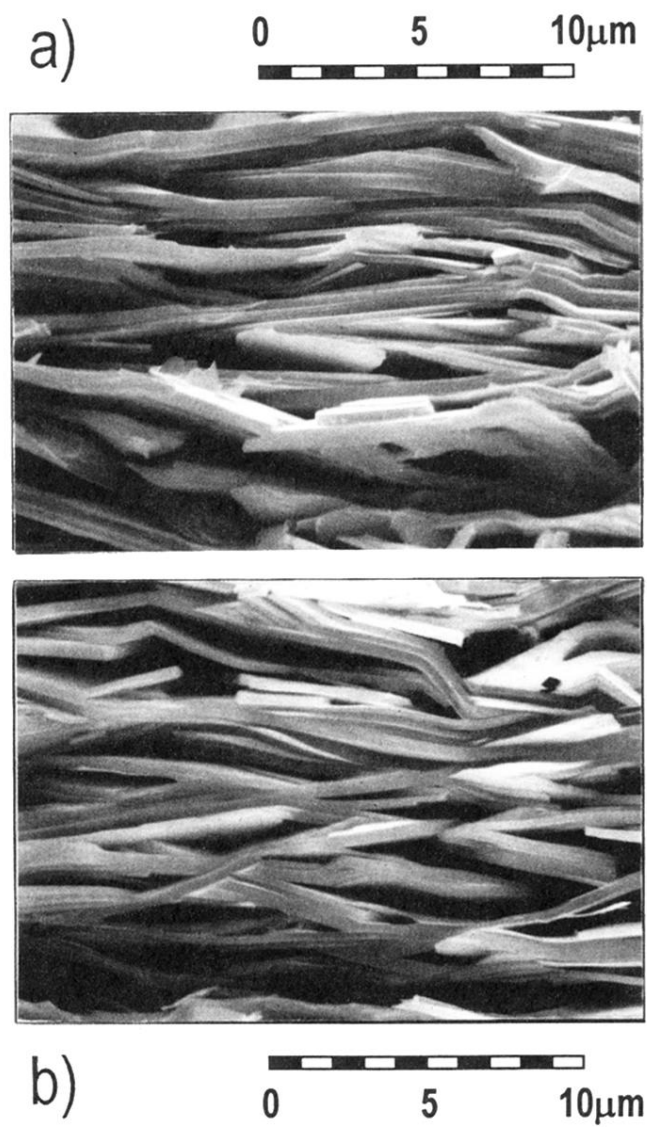
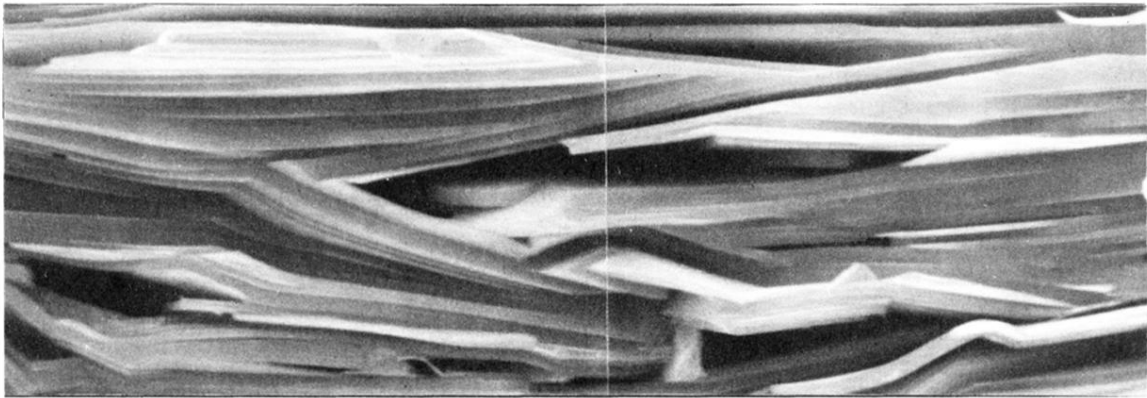


FIG. 3. Transverse (a) and longitudinal (b) fracture surfaces of a Bi/Pb (2223) filament with $j_c(T=77\text{ K}, B=0\text{ T})=25\text{ kA/cm}^2$ (SEM). The fractures were taken in the middle of the filament and span approximately half of the total filament thickness.



0 5μm

FIG. 4. A typical railway-switch network in a Bi/Pb (2223) filament (same tape as in Fig. 3; SEM).

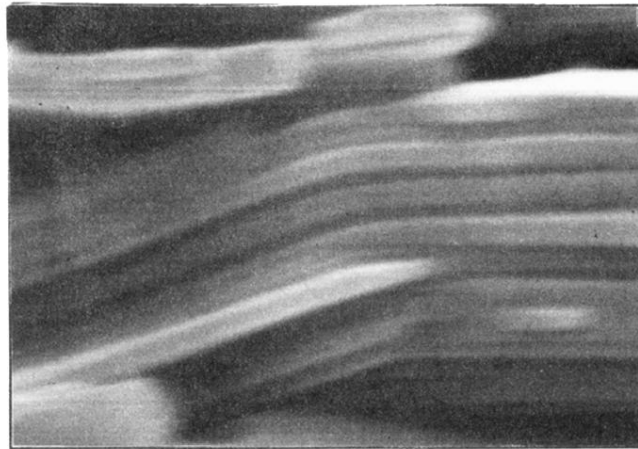
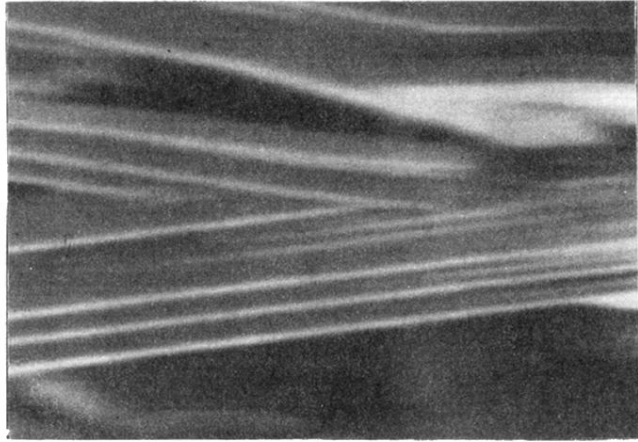


0 5μm

FIG. 5. Small-angle *c*-axis tilt (SCTILT) grain boundary connecting two Bi/Pb (2223) grains (SEM).

a)

0 1 μ m



b)

0 1 μ m

FIG. 7. Examples of SCTILT (a) and ECTILT (b) grain boundaries in Bi/Pb (2223) tapes (SEM). A series of ECTILT grain boundaries give the grains a softly bent or wavy shape (b).